PHASE EQUILIBRIA AND MAGNETIC CHARACTERISTICS OF RE-Co-Fe-Cu-Zr ALLOYS IN THE COMPOSITION RANGE OF RE : TRANSITION METAL $\simeq$ 1 : 7

A Thesis Submitted
in Partial Fulfilment of the Requirements
for the Degree of
MASTER OF TECHNOLOGY

by

M. UMA DEVI

to the

DEPARTMENT OF METALLURGICAL ENGINEERING

INDIAN INSTITUTE OF TECHNOLOGY KANPUR

JULY 1985

Dedicated to

My Parents

CERTIFICATE

This is to certify that this work on "PHASE EQUILIBRIA AND MAGNETIC CHARACTERISTICS OF RE-Co-Fe-Cu-Zr ALLOYS IN THE COMPOSITION RANGE OF RE : TRANSITION METAL $\simeq$ 1:7" by Mannem Uma Devi has been carried out under my supervision and that this has not been submitted elsewhere for a degree.

July, 1985

(Dr. K.P. GUPTA)
Professor
Dept. of Metallurgical Engineering
Indian Institute of Technology
Kanpur

ACKNOWLEDGEMENTS

I wish to express my deep sense of indebtness and gratitude to Dr. K.P. Gupta, Professor, Met. Engg., IIT Kanpur, who proposed, guided and helped this work to completion through his uncountable suggestions and constructive criticisms.

I am thankful to Dr.D.Bahadur and Prof.R.K. Ray for their kindness in allowing me to work in Magnetics lab. (ACMS) beyond office hours.

I am grateful to Dr. S.B. Rajendra Prasad for his immense help and nice company without his timely assistance the work would not have completed in time.

I am also thankful to Mr. V.P. Gupta, Mr. Uma Shankar, Mr.Agnihotri and Mr.B.K.Jain for their technical help in need.

Lastly but not the least thanks are also due to Mr.U.S.Mishra for his excellent typing.

-M. Uma Devi

TABLE OF CONTENTS

LIST OF TABLES

LIST OF FIGURES

PAGE

CHAPTER I

INTRODUCTION

A magnet is fundamentally an energy storage device. The energy is put into it when it is first magnetised and it remains in the magnet, if properly made and maintained, indefinitely i.e., the magnetism is permanent. The energy of a magnet which is chiefly the energy of its external field is always available for use and is not drained away by repeated use, because a magnet does no net work on its surroundings (1). For a permanent magnet the field strength in the gap between pole pieces of a permanent magnet (H_g) is given approximately by the relation,

$$H_g^2 = (BH)_{max} \left(\frac{V_m}{V_g}\right)$$

where V_m and V_g are the volumes of, the magnet material and the gap between pole pieces respectively and $(BH)_{max}$ is the maximum energy product of the magnet. For given volumes V_m and V_g, higher H_g may be obtained if the material used for magnet fabrication has high value of $(BH)_{max}$. Conversely, for a given H_g and V_g high value of $(BH)_{max}$ of a material will mean, requirement of smaller volume of magnet material. The requirement of energy saving as well as miniaturisation of devices employing magnets has generated in recent years a renewed interest in the research of new, high energy product magnet materials.

Wide spread interest in R-Co compounds dates from 1966, when Hoffer and Strnat (2) reported that YCo_5 had an anisotropy constant (K_1) of 5.5×10^7 ergs/cm^3, by far the largest value for any material then known. Since then it has been found that $SmCo_5$ has an even larger value of K_1, about 7.7×10^7 ergs/cm^3 which is more than 20 times that of barium ferrite. Properties of some RCo_x compounds and other important permanent magnet materials are given in Table I.1 (2).

Table I.1 : Magnetic Properties of Some Permanent Magnet Materials

Compound	Anisotropy Field H_A, KOe	Saturation Magnetisation $4\pi M_s$, KG	$_iH_c$ KOe	$(BH)_{max}$ MG Oe	T_c, °C
ALNICO-9	12.1		1.6	8.5	
Ba-Ferrite	17.0		3.1	3.1	
YCo_5	129	10.6	6.7	28.1	700
Ce Co_5	190	7.7	2.8	18.9	347
Sm Co_5	250	9.65	25	22.5	724
MM Co_5 (Ce based)	188	8.5	4.75	18.0	~500
Sm_2Co_{17}	80	12.0	2.0	36.0	~900

A high quality permanent magnet material must have the following properties (i) high saturation magnetisation (M_s) and remanance (M_r), (ii) high Curie temperature (T_c), (iii) uniaxial

anisotropy, (iv) large value of magneto crystalline anisotropy constant (K_1) or large anisotropy field (H_A) and (v) high coercive force (H_c). Besides these requirements, the material must have corrosion resistance, thermal stability and should be cheap. The first four properties depend on the material, its crystal structure etc. whereas the fifth property is a structure sensitive property.

The main contribution towards saturation magnetisation of RCo_5 compounds is made by parallel (i.e. ferromagnetically coupled) magnetic moments of the Co atoms. In addition to this, in the compounds with Y and light rare elements (La to Sm) the net magnetic moments of rare-earth atoms are parallel to those of the Co atoms. In compounds of the heavy rare-earths (Eu to Lu) the rare-earth magnetic moments are antiparallel to those of the Co atoms (3). Because of this, most of the work done with the RCo_5 type magnetic materials involve the light rare-earth elements. The RCo_5 alloys are with hexagonal crystal structure with uniaxial anisotropy (4) i.e., the easy direction of magnetisation is the [0001] direction.

The coercive field of a material depends on many factors. High coercive field in RCo_5 alloys is due to very large anisotropy fields varying between 190 KOe for $CeCo_5$ to 250 KOe for $SmCo_5$. The coercive field finally developed in a magnet is, however, influenced by many processing parameters. High coercive fields also can be developed by making conditions favourable in an alloy for

pinning domain walls. This approach has also been used in some rare-earth - cobalt base alloys(5). Examples of these are the Sm (Co, Fe, Cu, Zr)$_{7.5}$ and Ce-Co-Fe-Cu alloys. Yet another method to increase coercivity is by precipitating out elongated particles of magnetic phase in a nonmagnetic matrix thereby coupling high anisotropy field as well as shape anisotropy effect to yield high values of coercivity (as in $SmCo_3Cu_2$ alloys) (6).

The first R-Co permanent magnets were based on the RCo_5 compounds because they showed the best magnetic characteristics, high value of K and high T_c. Even though the $SmCo_5$ alloy showed the best permanent magnetic characteristics and magnets have been fabricated with $4\pi M_s$ = 9.65 KG, $_iH_c$ = 25 KOe and B_r = 9.5 KG (7), they are very costly because of the high price of Sm. One possible way of reducing the cost of RCo_5 magnets is to use less costly rare-earth elements like Ce or rather cheap Mischmetal (MM) by sacrificing to some extent magnetic characteristics (See Table I.1). Lately, Co has become a rare commodity. Attempts to replace some of Co by other transition elements, especially Fe, has shown that on addition of Fe, even though M_s increases to some extent, $_iH_c$ as well as $(BH)_{max}$ decreases considerably (8). In such cases addition of Cu along with other elements like Mg, Zr etc. appears to solve the problem because with these additions the alloys become magnetically hardenable through aging treatment (9). Even in these cases the studies made were restricted mainly to Sm alloys (5) (some work with Ce alloys have been reported also (10,11)) with a shift of composition from 1:5 stoichiometry towards

2:17 stoichiometry. Even though the magnets fabricated with the latter alloys are usually called the 2:17 type magnets, the best properties are found near about 1:7 stoichiometry. For the latter type of alloys so far no work has been done to replace rare-earth elements Sm or Ce by Mischmetal.

I.A Phase Equilibria

I.A.1 R-Co Binary Systems

Most of the light rare-earth elements show the same type of binary diagrams with modifications in their peritectic, eutectic and eutectoid transformation temperatures. A typical binary phase diagram of Ce-Co system (12,13) is shown in Fig.I.1. In this system as well as in most other systems the Co rich phases appear at the stoichiometric compositions of 1:2, 1:3, 2:7, 5:19, 1:5 and 2:17. Of these the alloys with high Co content, near 1:5 and 2:17 stoichiometries, appear to be important from permanent magnet point of view. The RCo_5 phase appears to decompose through an eutectoid reaction in most of the R-Co systems. The binary RCo_x phases of importance are indicated in Table I.2 (14). All the structure types of the phases existing at 2:7, 5:19, 1:5 and 2:17 stoichiometries are related to each other as they can be derived from the $CaCu_5$ type structure through simple substitution accompanied by layer shifts (15).

The Ce base MM-Co system has been studied by Schafer and Spyra (16) and Velu et al (17). In the composition region of 2:7 and 2:17, MM-Co phase diagram appears very similar to the Ce-Co

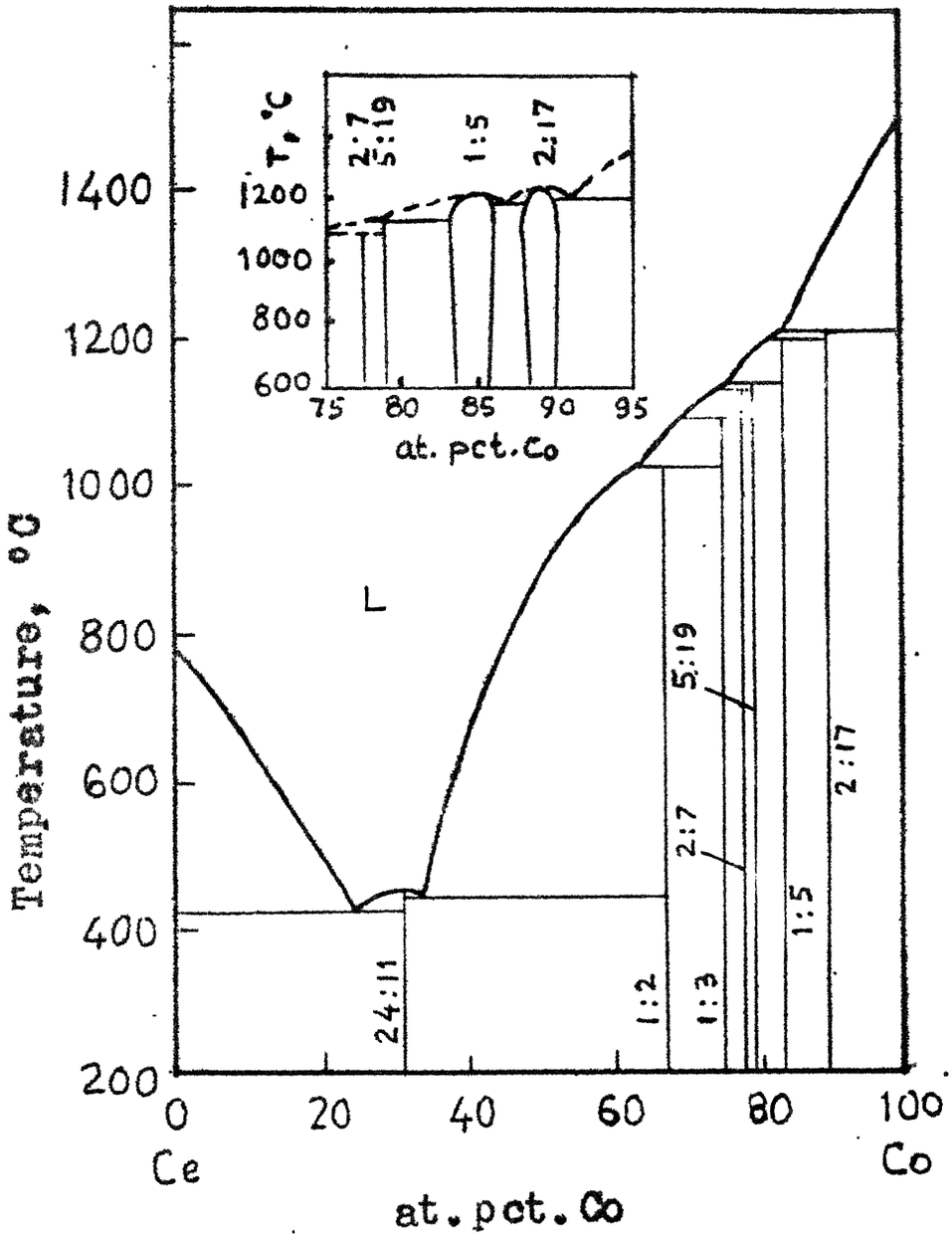

Fig.I.1 : Ce-Co phase diagram.

diagram. All the binary phases 2:7, 5:19, 1:5 and 2:17 were found to occur in the MM-Co system and $MMCo_5$ alloy was also found to decompose through an eutectoid decomposition (16,17). Since Velu et al (17) used Indian Mischmetal containing ~6 wt. pct. Fe, it appears that at least this amount of Fe has no drastic effect on the nature of the phase diagram which is given in Fig.I.2.

Table I.2 : Crystal Structures of $R\text{-}Co_x$ Compounds (14)

Compound	R	Lattice symmetry	Structure type
R_2Co_7	La, Ce, Sm, Pr, Gd	Hexa.	Ce_2Ni_7
	La, Ce, Gd, Tb, Pr	Rhombo.	Gd_2Co_7
R_5Co_{19}	La, Ce, Pr, Nd, Sm	Rhombo.	Ce_5Co_{19}
	Ce, Sm, Nd, Pr	Hexa.	Sm_5Co_{19}
RCo_5	La, Ce, Sm, Pr, Nd, Gd, Tb, Dy	Rhombo.	$CaCu_5$
R_2Co_{17}	Ce, Pr, Nd, Sm, Gd	Rhombo.	Th_2Zn_{17}
	Y, Tb, Dy, Ho, Er, Tm, Yb, Lu	Hexa.	Th_2Ni_{17}
RCo_{13}	La	Cubic	$NaZn_{13}$

I.A.2 The RE-Co-Fe Ternary System

Recently phase equilibria at 900°C has been studied in the MM-Co-Fe system using Indian MM (18). The phase equilibria at 900°C has been represented as RE-Co-Fe system (Fig.I.3) (19) by

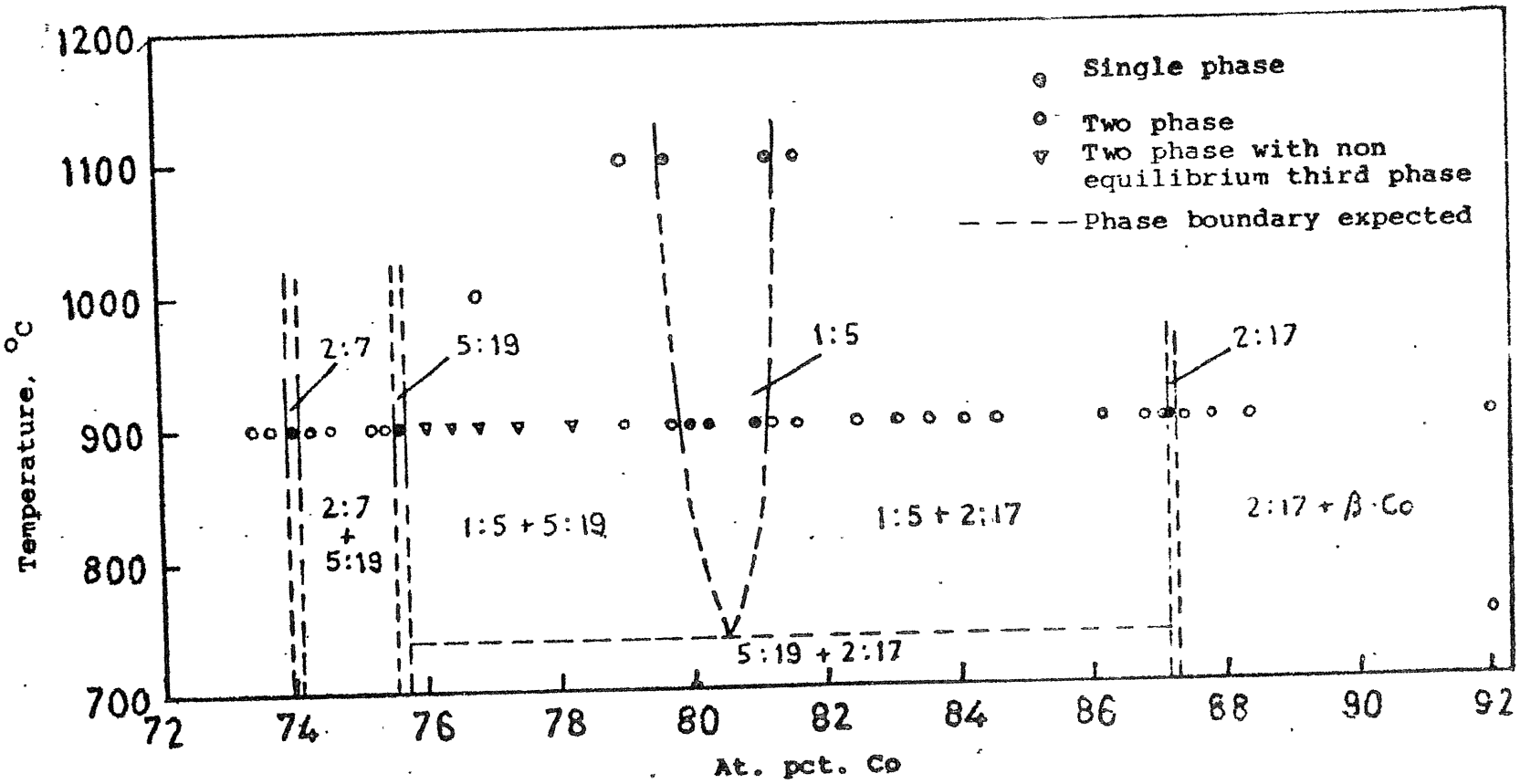

Fig.I.2 Indian MM-Co phase diagram.

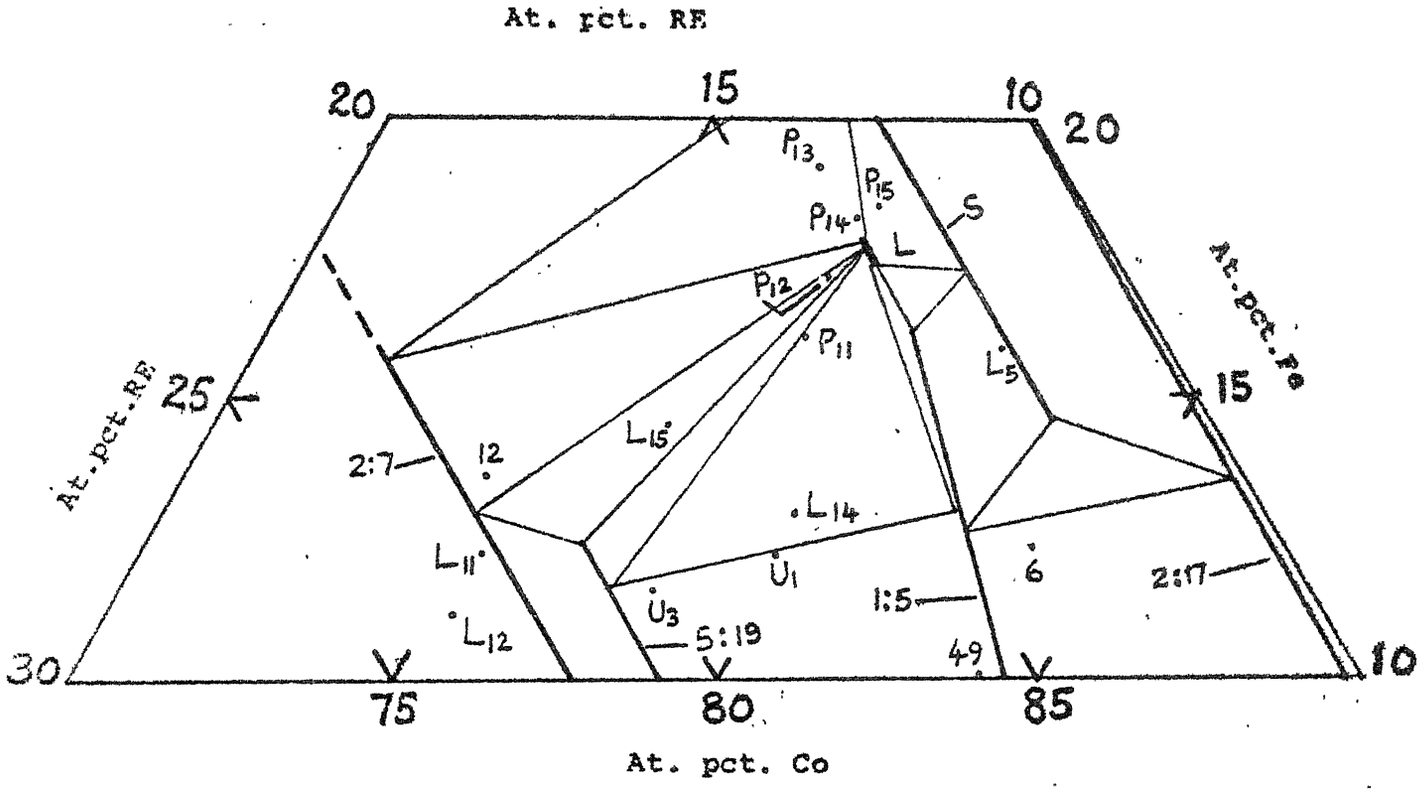

Fig.I.3 A part of 900°C isothermal section of RE-Co-Fe system.

considering the total rare-earth content of MM as RE and Fe represents the total iron content of the alloy. Besides the extension of the binary 2:7, 5:19, 1:5 and 2:17 phases into the ternary, four new ternary phases were found to occur in the RE-Co-Fe system, two of which L and S have been shown in Fig.I.3 and the other two phases A and T appear at much higher Fe contents. Of these binary (RE-Co) and ternary phases the 1:5 and the S-phase were found to possess uniaxial anisotropy, high T_c and high M_s and hence are important as permanent magnet material. It should be noted that the S phase appears close to the 1:7 stoichiometry.

I.A.3 R-Co-Cu Ternary System

The isothermal sections of Sm-Co-Cu phase diagram reported by Perry et al (20) at 800°C and 1200°C are shown in Fig.I.4a and I.4b. It is seen from Fig.I.4a that at 800°C, $SmCo_5$ and $CuCo_5$ are completely miscible in each other. The Sm_2Co_7 phase extends into the ternary upto about 38 at. pct. Cu but, the $SmCo_3$ and Sm_2Co_{17} phases extend only upto a few at. pct. Cu into the ternary. At the Co end of the diagrams two narrow three phase regions containing 1:5 + 2:17 + γ (fcc) and 2:7 + 1:5 + 2:17 exist at 800°C. However, the three phase regions vanish at 1200°C.

Velu (21) studied the R-Co-Cu system by replacing completely the pure rare-earth element (R) by MM. This study was restricted to the 1:5 stoichiometric alloys annealed at 900°C.

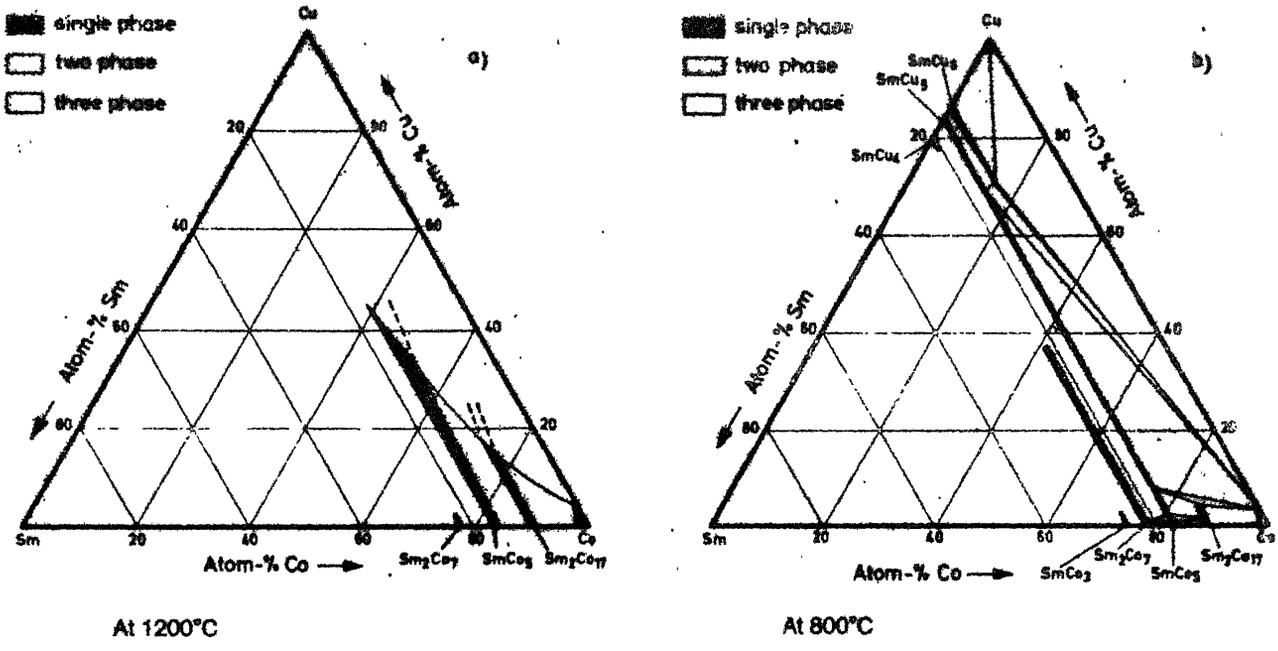

Fig.I.4a,b : Isothermal sections of the Sm-Co-Cu phase diagram.

All the alloys were found to posses more than one phase (possibly due to shift in alloy composition). At the Co rich regions the alloys $MM(Co_{1-x}\ Cu_x)_5$ with $0 < x \leq 0.2$ showed the presence of 2:17 phase in a matrix of 1:5 phase. A small amount of a third phase, which could not be identified, was also present (The amount of 2:17 phase was found to increase at 700°C). For $x \simeq 0.3$ the phases present were 1:5 and the unidentified phase. For $0.4 \lesssim x \lesssim 0.6$ the phases in equilibrium were 1:5 and γ (fcc) and at the highest Cu contents the phases in equilibrium were 1:5 and 1:6. The results thus suggest that a complete series of solid solution exist between $MMCu_5$ and $MMCo_5$.

I.B. Magnetic Characteristics of RE-Co-Fe-X Alloys

Magnetic properties of R-Co, RE-Co-Fe alloys are discussed in the earlier sections. In this section magnetic characteristics of RE-Co-Fe-X alloys are reviewed where X either represents a single transition element or more than one element of which some are transition elements and some nontransition elements.

Among the recently developed RCo_5 based permanent magnets, the Cu containing alloys developed by Nesbitt et al. (6) are of particular interest. These alloys are age hardenable type (9) i.e. their magnetic properties are improved and controlled by suitable heat treatment. Aging treatment usually produces fine scale precipitation or separation of ferromagnetic RCo_5 and nonferromagnetic RCu_5 on fine scale. Addition of Cu, causes M_s to go down. Since Fe raises the M_s of RCo_x phases, Fe is added to

$R(Co, Cu)_5$ system to compensate for the decrease in M_s. This principle has been used in the development of Ce $(Co, Fe, Cu)_5$ magnet materials (10, 11). $_iH_c$ has been found to depend on the Cu content, aging temperature and aging time.

Practically no data is available for the MM $(Co, Fe, Cu)_5$ alloys. Some work done at IIT Kanpur on these alloys (21) show that magnetic properties of the sintered magnets are rather poor, possibly due to the presence of the 2:17 phase and due to oxidation of fine powder.

From the recent work of Walkiewiez and Wong (22) on MM $(Co, Fe, Cu, Mg)_5$ alloy it has been found that there is a large improvement of magnetic properties compared to the $Ce(Co, Fe, Cu)_5$ alloys. These Mg containing MM alloys have the following magnetic properties: $_iH_c$ = 29 KOe, $_BH_C$ = 5.890 KOe, B_r = 6.900 KG and $(BH)_{max}$ = 10.3 MGOe.

During the last few years, the focal point of research and development in the field of RE : transition metal magnet materials has shifted from 1:5 to the so called 2:17 alloys. The more appropriate stoichiometry of the alloys studied is near 1:7. In these alloys the final improved permanent magnet property is developed only through aging. These are Sm based alloys with partial replacement of Co by Cu and Fe and small alloy addition of Zr, Hf, Ti, Mg etc. (23-26).

Influence of decomposition of supersaturated solid solution on the coercive force of $Ce(Co_{0.75}Fe_{0.11}Cu_{0.13}Ti_{0.01})_6$

with aging has been studied by Arbuzov et al (25). With rise in temperature, the value of coercivity was found to increase at first reaching a maximum at 497°C and then decreasing.

Among all the constituents studied till now Zr seems to be the most effective for permanent magnet application. The most important alloy has five components Sm, Co, Fe, Cu and Zr. In order to understand the role of Zr the ternary alloys $Ce_2Co_{17-x}Zr_x$ and $Sm_2Co_{17-x}Zr_x$ have been studied. Crystallographic and magnetic characteristics indicate that Zr replaces Co when the ternaries are formed. T_c and saturation magnetisation appears to decrease and the anisotropy field, H_A, appears to increase significantly with increase in Zr content.

In the case of Sm-Co-Fe-Cu-Zr alloys the magnetic properties were obtained for sintered magnets (27) after aging at 800°-850°C for 10-30 hrs, following the solution treatment at 1150°C and subsequent step aging (continuously cooled to 400°C at a cooling rate of 1-2°C/min. and then aged at 400°C for 10 hrs.) Here the best hard magnetic properties of $(BH)_{max}$ = 33 MGOe and $_iH_c$ = 13 KOe were obtained for $SmCo_5Fe_{2.17}Cu_{0.38}Zr_{0.13}$ alloy.

It has been shown (28) that the coercivity mechanism in these alloys can not be explained on the basis of the difference of magneto-crystalline anisotropy constants K_1 of matrix and the precipitate phases only. However, it has been suggested (28), that the coercivity may be described by the decrease in the domain wall energy at the precipitate, resulting in an attractive

interaction between the precipitate and the domain wall. A honeycomb structure (29,30) involving a close meshed network of 1:5 phase around the 2:17 phase regions was detected under electron microscope. In the alloy Sm $(Co_{0.8}Cu_{0.15}Fe_{0.05})_7$ (30) the composition of the matrix was found to be $Sm(Co_{0.78}Cu_{0.18}Fe_{0.05})_{7.5}$ (2:17 type phase) and that of the precipitate was $Sm(Co_{0.74}Cu_{0.22}Fe_{0.05})_{6.4}$ (1:5 type phase). A $(BH)_{max}$ of 20-30 MGOe, B_r = 11-12.5 KG, $_BH_C$ = 5-5.4 KOe were reported for $Sm(Co_{0.69}Fe_{0.2}Cu_{0.1}Zr_{0.01})_{7.4}$ after a multistage heat treatment (31).

I.C Fabrication Methods

The earliest method used for fabrication of the rare-earth-cobalt magnets was by directional solidification of the liquid alloy in analogy with the Alnico manufacturing technology where during cooling rod like precipitates form parallel to the cooling direction. The cause of magnetic hardness is shape anisotropy. However, the casting approach ran into insurmountable practical difficulties and is ruled out now.

The most commonly used technique for producing rare earth-cobalt magnets is through the powder metallurgy route. In this process the alloy is powdered, pressed to shape and sintered to form the magnets. The starting material is often pure metals melted in arc or induction furnace to form the alloy of suitable composition. The other possible variation is the formation of alloy from the pure oxides of components through co-reduction process.

In the latter case the alloy is obtained in fine powder form and hence comminution steps are reduced. Industrial production methods follow classification and blending of powders to get a narrow size distribution of fine powders. The powders are made into compacts of required size under magnetic field so that all the fine particles orient their easy direction of magnetisation along the applied field direction. Then the important stage is sintering of these green bodies to increase their density. It could be solid state sintering (32) or liquid phase sintering (33). In liquid phase sintering, the alloy powder is taken first at off stoichiometry and a low melting point, high rare-earth content alloy powder is added and sintered. The low melting point powder melts and fills the gaps and alloys with the high melting powder particles of the compact to shift the stoichiometry of the final alloy to the right value. By this method higher density sintered magnets can be made. A post sintering heat treatments is usually given to the sintered magnets to improve their magnetic properties. The steps followed in industrial practice of fabrication of Sm-Co magnets are given in the flow diagram of Fig.I.5 (36)

I.D Statement of the Problem

For the development of the permanent magnets a continuous search for materials with good magnetic characteristics has been going on for the past several years. RE-Co alloys represent a family of magnets with the best known permanent magnet characteristics so far and interest in these materials has

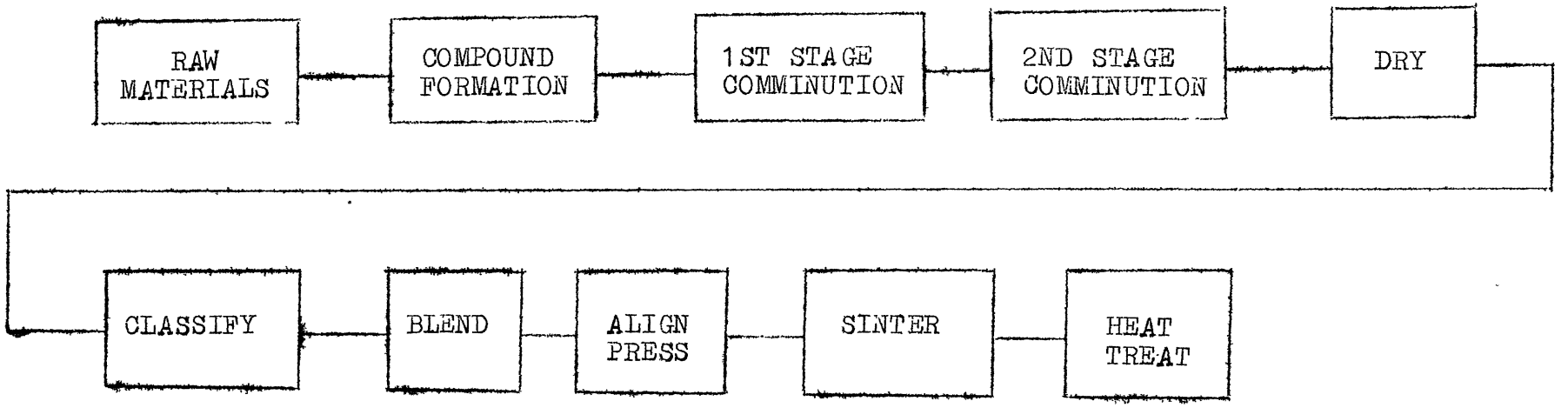

Fig.I.5 Process Flow Diagram for Sintered Rareearth-Cobalt Permanent Magnets (36)

increased in recent times. In this respect $SmCo_5$ was found to give excellent magnetic properties. Due to the scarcity and cost of Sm and scarcity of Co the $SmCo_5$ magnets have not become that popular. Nevertheless it has become increasingly apparent that not all properties of a permanent magnet are equally important for a given application. So that the potential of these $SmCo_5$ magnets is not always completely utilised. Hence, it has became desirable to widen the variety of RE-Co magnets by developing new types, of alloying with various transition and nontransition metals.

Recently, however, tremondous improvement of magnetic properties has been achieved through the discovery of Sm(Co,Fe,Cu, $Zr)_7$ type magnets. Since pure Sm is very costly, a relatively cheap mischmetal (MM) can be used in its place. No work in this direction has been reported so far.

India has large deposits of rare earths and MM is cheap. It has not been possible to utilise these mischmetals to fabricate very good permanent magnets of the $MMCo_5$ type or $MM(Co,Fe)_5$ type for which the magnetic property is dependent on the inherent characteristics of the material. Since in the 1:7 type magnets the properties are enhanced by aging and possibly not so much dependent on the inherent characteristics of the alloys, it is probably possible to replace Sm by MM completely or partially in fabricating 1:7 type magnets. With this in mind the preliminary work on MM(Co-Fe-Cu-Zr), alloy has been started. Since fundamental

understanding of the behaviour of alloys need the knowledge of phase equilibria, in this investigation it was considered appropriate to devote reasonable amount of time to understand the phase equilibria in the complex multicomponent system around the rare-earth : transition metal ratio of 1:7. Investigation of the RE-Co-Fe-Cu-Zr system around the 1:7 stoichiometry (stoichiometry varying from 1:4.75 to 1:18) keeping Cu and Zr levels constant at 8 and 2 at. pct. respectively and Fe content varying from 10.75 to 18.75 at. pct. has been contemplated. Study of phase equilibria will be done using the metallographic and X-ray diffraction techniques. Since the phases present in the RE-Co-Fe system give rather similar X-ray diffraction pattern but have reasonably different Curie temperatures, thermomagnetic analysis will be employed for phase identification.

As a first step in the fabrication of magnets with these alloys, it is proposed to determine some process parameters that may lead to better magnetic property of the material.

CHAPTER II

EXPERIMENTAL PROCEDURE

The present investigation involved a limited amount of study of phase equilibria in the system MM-Co-Fe-Cu-Zr at fixed levels of Cu and Zr and characterisation of the alloys for the purpose of development of hard magnets. The experimental procedures followed and the techniques used for characterisation are as described in the following sections.

II.A Alloy Preparation

II.A.1 Materials Preparation

Alloys were prepared using Indian mischmetal (cerium rich), cobalt, iron, copper and zirconium. Commercial mischmetal supplied by Raw Flints Pvt. Ltd., Rajkot, Gujarat, has the following composition : 87 wt. pct. RE, 12 wt. pct. Fe and 1 wt. pct. impurities. An effective grain atomic weight for that mixture of rare earths is 140.09 gms computed, on the basis of X-ray fluorescence analysis of rare earth elements in MM. Cobalt, iron and copper supplied by Semi Elements, Inc. New York, USA, were of 99.9 pct. purity. Iodide zirconium with purity 99.9 pct. was also supplied by Semi Elements, USA.

Commercial mischmetal was in form of biscuits dipped in some heavy oil to protect them from atmospheric oxidation. The small pieces of mischmetal were cut using a saw and the

oxide player from the surface of the cut pieces was removed by grinding and stored in toluene. Cobalt, in the form of cast buttons was cut into small pieces and the surface was polished. Electrolytic iron was in the form electro deposited flakes and its surface was ground to remove oxide layer. Copper was in the form of small nodules. The pieces of all these metals were weighed accurately according to the chosen composition of the alloy so as to make the total weight of the alloy to be 10 gms, or 20 gms as was needed.

II.A.2 Melting of Alloys

Melting of the alloy was done in a non-consumable tungsten electrode d.c. arc furnace on a water cooled copper crucible. A definite charging sequence was followed,so as to have uniform melting losses in all the alloys. Low melting point metals were kept at the bottom and high melting point metals were at the top. The chamber was evacuated to ~50 microns of Hg pressure and flushed with ultra pure argon gas. This is repeated twice to remove oxygen present in the melting chamber and finally melting was carried out under argon atmosphere. Arc current was set between 300-500 amps at 40 volts. A melting time of 30 sec. was used. For proper homogenisation, each alloy was remelted at least three times after breaking the alloy button into pieces and putting them upside down on the crucible. The total loss in melting was always less than 1 wt. pct., usually in the range of 0.5 pct. Since the melting

losses were small the alloys were not chemically analysed. Alloys after melting were stored in a desiccator for further analysis.

II.A.3 Homogenisation and Annealing of Alloys

As the molten alloy was cooled very fast, seggregation is possible. To homogenise the alloys, the as cast alloy buttons were sealed in evacuated ($\sim$ 20 μ Hg pressure) quartz tube, annealed at 1100° $\pm$ 1°C for 2 days and water quenched to retain the equilibrium structure corresponding to 1100°C.

II.B Phase Analysis

II.B. 1 Metallography

A small and representative portion of the annealed alloy was taken for metallographic analysis. Annealed piece of an alloy was broken into two parts using a chisel and the freshly fractured surface of the alloy piece was selected for metallographic investigation. The chosen surface of the broken alloy piece was ground flat using a belt surfacer. Alloys were very brittle and hence careful specimen handling was necessary to prevent loss of particles during polishing operation. The ground piece of alloy was mounted in trans-optic powder using 'Simplemet-II' mounting press. The mounted specimen was polished successively on 1/0 through 4/0 emery paper taking care that no deep scratches are produced during polishing. The specimens were thoroughly washed in flowing water and subjected to rough polishing. Rough polishing was done on a rotating wheel covered with selvyt cloth.

1μ size alumina powder suspended in distilled water was used as a polishing abrasive. After polishing the specimen to some extent it was washed in running tap water and dried by using a high speed air blower. The final polishing was carried out on a 'Vibromet' polisher to produce scratch-free surface for metallographic analysis. To reveal the microstructures polished specimens were etched with dil. HNO_3 of various strengths, strength varying between 1 pct. to 6 pct. by volume. Time of etching varied from 2 swabs to 10 swabs depending on the composition of the alloy specimens. Microstructure of the specimens were observed using Zeiss Universal Metallograph.

II.B.2 Microhardness Tests

Microhardness of the individual phases had been measured in the case of a few alloys using Leitz Wetzlar microhardness instrument, to differentiate between phases which looked alike. Since this investigation was similar to microscopic investigation, the condition of the surface was of primary importance. Surface preparation similar to that described in Section II.A has been followed. Since in the present study the differences in hardness between the various phases present in a specimen are to be determined, the specimen was etched to reveal the structure and the indent was made well within the grain boundary of each phase so that the hardness value obtained did not have any influence due to its neighbouring grains. The hardness values are given in vickers hardness number

$$H_v = 189 \times 10^3 \times \left(\frac{F}{d^2}\right)$$

where F is the applied load given by F = 5P = 4903 milli Newtons and d is the width of indentation (in units of μm). Microhardness of each phase was measured on many grains of a phase and the average value was calculated.

II.B.3 X-ray Diffraction

For identification of different phases existing in each alloy a piece of each annealed alloy was carefully ground to remove the surface oxide layer and crushed in steel and agate mortars to -250 mesh size. Since the majority of the alloys were brittle, the as powdered alloy was used to obtain their diffraction patterns. In the case of high Co content alloys, the powders were stress relieved at 1100°C for 5 minutes and water quenched. The stress relieved powders were used for indexing diffraction patterns of different phases. To take diffraction pattern from a powder specimen the powder was packed in a perspex holder. Two to three drops of methanol was added to prevent the dry powder from falling out of the specimen holder. Diffraction patterns were taken using a Rich. Seifert Iso-Debyeflex 2002 D. Diffractometer. Cr-radiation and slow scanning speeds were used for better resolution. A graphite monochrometer was used in the path of the diffracted beam to eliminate scattered radiation and to remove Cr-K_β diffraction lines. Thus practically background free, β-radiation free, high resolution diffraction patterns could be

taken for phase analysis. Conditions set for taking diffraction traces are given in Table II.1.

Table II.1 : Conditions Set for Tracing Diffraction Patterns Using ISO Debyeflux 2002D . Diffractometer

Radiation	Cr unfiltered
Tube voltage	40 KV
Tube current	30 mA
Receiving slit width	0.2 mm
X-ray slit width	2 or 3 mm
Scanning speed	1.2°/min. (0.6°/min. in some cases)
Chart speed	15 mm/min.
Time constant	3 sec.
Intensity range	200 counts/sec.
Angular range of scan	$35° \leq 2\theta \leq 152°$

II.B.4 Thermomagnetic Analysis

Thermomagnetic analysis has been carried out using a simple, fabricated equipment (34) consisting of a furnace assembly capable of going to ~1100°C and a suitable detector system consisting of a transducer to provide a signal during change in the magnetic characteristics of an alloy with temperature, an instrument to amplify and process the signal to make it

suitable for recording.

II.B.4a Furnace Assembly

The furnace assembly is shown in Fig.II.1. It consists of a small furnace 1" dia. x 2½" long alumina tube wound with 22 gauge Kanthal-A heating element, supported on a water cooled brass plate and refractory insulating brick supports. Two radiation shields, inner one of stainless steel sheet and the outer one of aluminium sheet, surrounded the furnace. The top covers of radiation shields made of stainless steel and mild steel have 3/4" dia. holes at their centres through which the specimen holder can be inserted into the furnace. The whole assembly is covered by a water cooled brass cover with two sight holes at appropriate locations to monitor the movement of the specimen holder through the radiation shields. The brass cover is fitted at the top with a 1" dia. pyrex glass tube around which the transducer is placed. The tube ends in a top flange fitted with an O-ring seal through which the specimen holding arrangement operates. The specimen holder assembly consists of a brass tube, fitted with a copper sleeve, which can be screwed on to the tube end to hold the quartz tube specimen holder. Through the brass tube, which is fitted with an O-ring seal at the top, a 1/8" dia. thermocouple sheath carrying a Pt vs Pt + 10 pct. Rh couple is inserted into the quartz tube specimen holder. The inner diameter of the quartz tube specimen holder is ~ 6 mm. The tip of the thermocouple is positioned at the centre of the powdered specimen

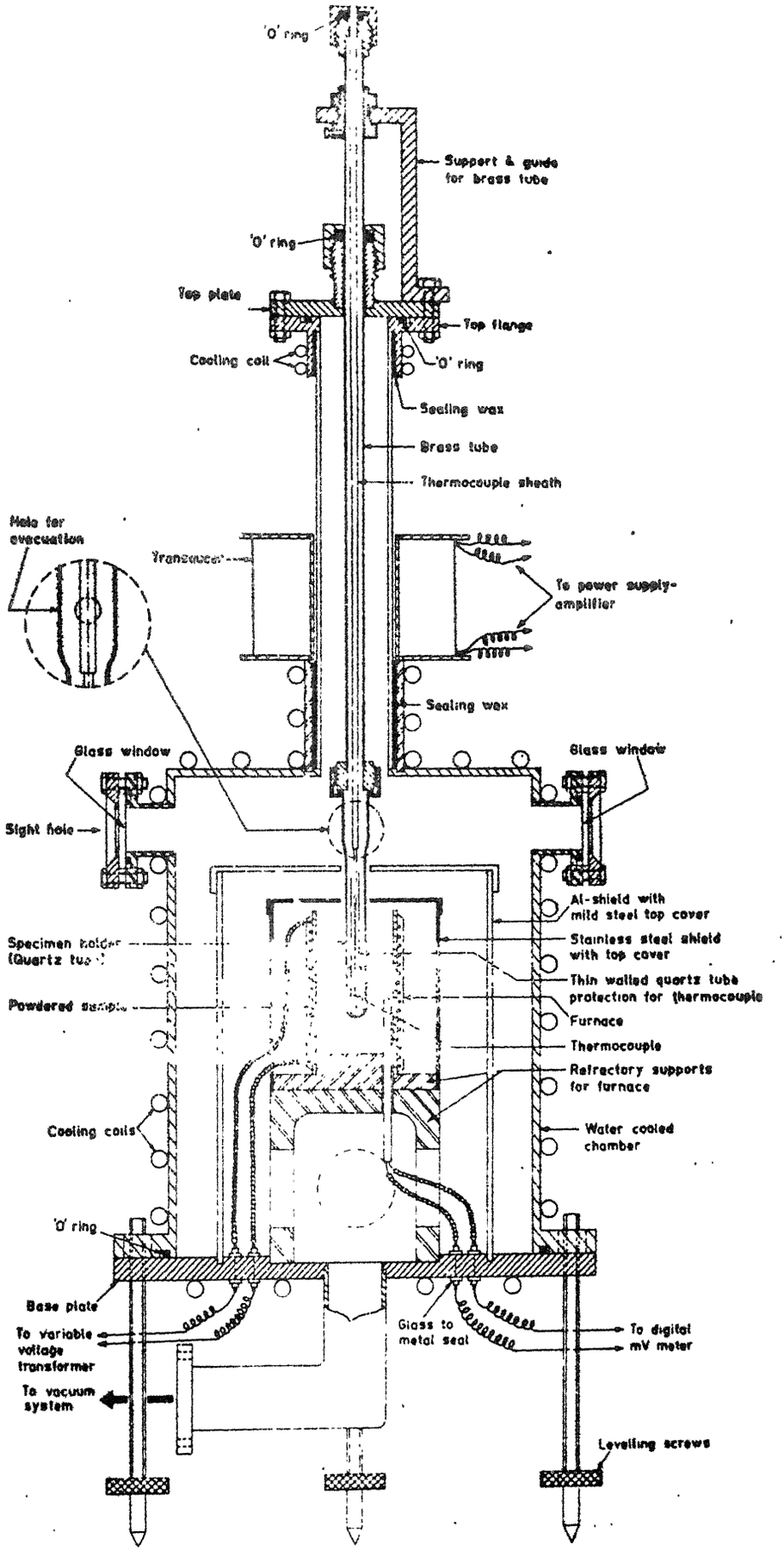

Fig.II.1 : Curie-temperature apparatus, furnace assembly.

and is protected from the specimen by a closed end thin walled quartz tube. The other end of the thermocouple sheeth is sealed off with quick fix. -250 mesh powder is used as specimen. Because of the small height of the transducer coil, the maximum permissible height of powder in the quartz tube specimen holder is about 1.4 cm. The bottom support plate has provision for connecting the furnace chamber with a vacuum system. The power leads for the furnace and a furnace temperature monitoring thermocouple (Pt vs Pt + 10 pct. Rh) are fed through glass to metal seals attached to the bottom support plate. Since the electrical resistance of the furnace is small, 1050°C can be reached at ~52V, power input to the furnace is controlled through two variable voltage transformers.

II.B.4b Detector System

The block diagram of the detector system is shown in Fig.II.2. The transducer employed is based on reluctive transduction principle and is essentially a differential transformer so that even a very week signal due to magnetic transformation of a weak ferromagnetic phase can be reliably detected.

In the absence of a sample, the coupling of the primary coil to both the secondary windings is the same. When a ferromagnetic sample with a temperature greater than its Curie temperature is inserted within the coil (Fig. II.2) the coupling with one of the secondary coils is maximum while for the other it remains more or less unchanged. As the sample cools down and passes

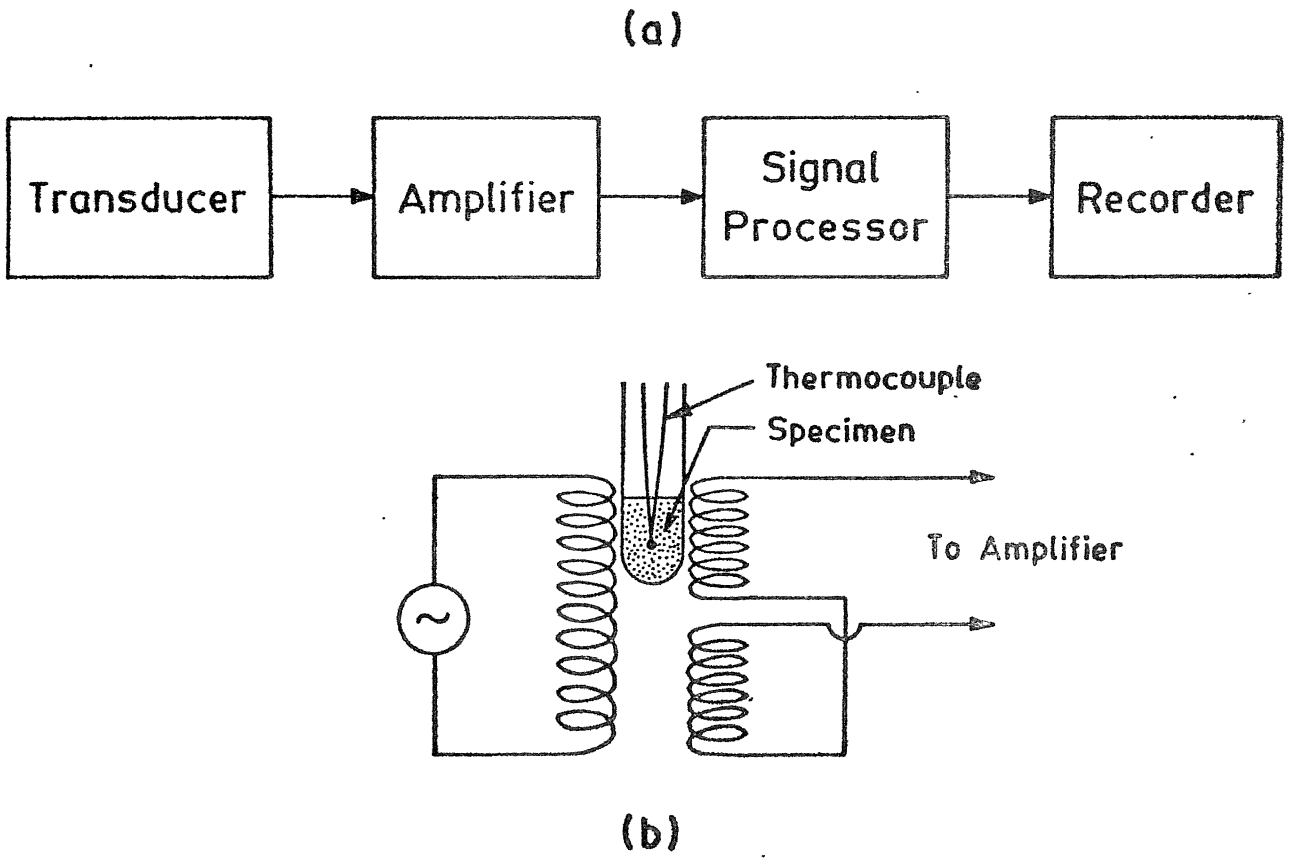

Fig.II.2 : Block diagram of detector system and differential transformer transducer with sample.

through Curie temperature, the reluctance of the path in one coil changes, causing change in the a.c. voltage out put. The output is connected to an amplifier through shielded wires to cut down the stray pick up in electrically hostile environment such as with electric furnaces, vacuum pumps etc., running beside the detector system.

The amplifier stage uses a very low drift high fixed gain, temperature compensated differential input-differential output operational amplifier at input, cascaded with another operational amplifier.

The signal processing stage consists of a multigain amplifier and a precision a.c. - d.c. conversion, filtering and zero elevation circuit. The multigain amplifier is switch selectable so that maximum amplification can be achieved without saturation setting in. Three different gains low (C), medium (M) and high (F) with gains 6, 60 and 600, respectively, can be selected depending on the type of material to be investigated. A final stage in signal processing provides zero elevation. This is useful when a sample consists of phases which are strongly and weakly ferromagnetic. When a strong signal is produced due to magnetic transition of a strong ferromagnetic phase the recorder will be almost at its maximum and with that sensitivity, the weak signal from a weak ferromagnetic phase is likely to be missed. By deviating the zero, the effective input to the recorder is reduced and thus higher sensitivies can be selected resulting in

clear identification of weak ferromagnetic phases.

An ordinary X-Y recorder available as a standard equipment may be used to get a continuous trace of permeability against temperature. The transducer is of active type and thus required external excitation. For better sensivity the equipment is operated at a frequency of approximately 300 Hz. The equipment is mains operated and all the power supplies required have also been built into the system.

The special features of this instrument are:

(i) it is sensitive to detect minute amounts of magnetic phases due to the inbuilt selectable multigain amplifier.

(ii) provision to keep the sample far out side the furnace zone when the furnace is getting heated up.

(iii) capable of going to high temperature ($\sim$ 1100°C)

(iv) evacuation to better than 1 μ Hg pressure; so that oxidation of the sample at high temperature is avoided.

(v) since it has provision for fast heating of the specimen (6 to 7 mts.), low temperature transformation of phases can be avoided and simultaneously the specimen is stress relieved.

(vi) the cooling rate of the specimen is reasonably slow so that each magnetic transition in multiphase alloys can be detected.

(vii) weak signals from weak ferromagnetic phases can be detected since the transducer is a differential transformer and there is a xero elevation circuit.

(viii) total time taken to record the trace is 10-15 mts. and hence the magnetic transition temperature may be determined repeatedly to verify the result of one test.

II.B.4c Magnetic Test Procedure

The change in permeability during magnetic transition is not same for all phases. For strongly ferromagnetic phases the amount of powder taken has to be controlled so that no saturation occurs. In the high cobalt side of RE-Co-Fe base alloys the height of powder taken in the quartz sample holder was ~ 0.7 cms (~0.5 gms) and for high RE side alloys it was ~ 1.4 cm.

To detect the magnetic transition of a given specimen the furnace chamber is first evacuated to better than 10^{-4} mm Hg pressure using rotating and diffusion pumps and the furnace is heated up slowly to the required temperature. During this period the specimen is kept far away from the furnace. On achieving appropriate furnace temperature the specimen holder is lowered to put the specimen tube in the hot zone of the furnace. The specimen takes only 6 to 7 mts. to heat up to the furnace temperature. On reaching a stable specimen temperature the specimen tube is quickly withdrawan into the transducer coil section and allowed to cool. The specimen temperature and the output of the detection system are recorded on a Hewlett-Packard X-Y recorder. Details of

operation of the permeability apparatus is given in Appendix-I.

II.C Magnetic Characterisation

The particular properties of interest for a permanent magnet are saturation magnetisation, M_s, remenance, M_r, and coercivity, H_c. It is also of interest to see how $_iH_c$ gets affected by aging and what variation in the process variables will result in better magnetic property when magnets are produced following the powder metallurgy route. In order to get these information tests were carried out on bulk specimen as well as resin bonded powder magnets. The procedure followed for these tests are described below.

II.C.1 Low Temperature Aging

The 1100°C annealed alloys pieces of magnetically important alloys (close to 1:7 stoichiometry) were sealed in evacuated fused silica capsules and aged at three temperatures, 675°C, 650°C and 620°C, for various lengths of time and their magnetic characteristics, $_iH_c$ as well as M_s were measured as a function of time at intervals of 10 hrs. annealing and in one case after about 100 hrs. annealing period.

II.C.2 Magnetic Measurements

A PAR 150 A Vibrating Sample Magnetometer was used for measurement of $_iH_c$, M_s and M_r/M_s ratio. The principle of the magnetometer is described below in brief.

A small sample of the material whose magnetic moment is to be measured is placed in a sample holder. The sample holder is mounted on the end of a rod and suspended and vibrated in the field of the superconducting magnet.

The sample is vibrated in a uniform magnetic field by means of a transducer at a fixed frequency and a fixed amplitude. The induced field in the sample induces a emf in a pair of stationary pick up coils. The induced emf is amplified by a suitable electronic circuit and converts it into magnetic moment in electromagnetic units (emu).

The system is calibrated using the 3/32" dia.x 3/32" long cylindrical sample of high purity Ni for which the saturation moment is 55 emu/gm. The sample is mounted between the electromagnets in a perspex sample holder and is aligned and adjusted there by locating it symmetrically with respect to the detection coils. The main benefit of making this adjustment is that the different samples were adjusted to the same position relative to the pick up coils, thus minimizing the effect of geometry on the results of measurement. The sample is first taken to saturation by increasing the field strength (H) of the electromagnet to its maximum value (10 KOe) where the magnetometer panel meter reads the value of M_s in emu. The field strength is then decreased to zero and the value of M_r is noted from panel meter. Field direction is then reversed and the field strength is increased slowly till the panel meter reads zero. The present model of VSM is having provision for stepwise increase (or decrease) of field strength,

a continuous variation of field strength is not possible. Hence finding $_iH_c$ accurately at once was difficult. To overcome this difficulty at first the field strength, in the reverse field mode, was increased in larger steps of 100 Oe. Once the approximate location of $_iH_c$ was found the specimen was again remagnetised by 10 KOe positive field. During demagnetisation process, in the reverse field mode, demagnetisation was done in smaller steps of 10 Oe in the critical range of field strength so as to make the magnetisation go to zero. The same procedure was repeated a third time so that in the critical range of field strength a decrease by 1 Oe field strength was used. From this data $_iH_c$ was determined by plotting M vs -H.

II.D Setting up of Some Parameters for Magnet Fabrication

The most important factors for magnet fabrication are alloy composition, oxygen content, powder particle size and size distribution, aligning field, sintering and heat-treatment cycles to maximize the $_iH_c$ and to optimize overall second quadrant magnetic characteristics. Instead of studying each parameter in detail a shorter route was followed and is described below.

Large size particles tend to be multigrained and do not align or sinter properly. Undersized particles pick up an excessive amount of oxygen which reacts with the metallic components to form oxide resulting in an overall shift of the composition out of the range where optimum properties are achieved. In order to determine optimum powder characteristics for magnet fabrication

an alloy may be ground and fabricated into a resin bonded magnet to determine the magnetic characteristics. This may be done at various stages of grinding so as to determine the optimum grinding time needed for a given alloy. The procedure followed for making resin bonded magnets is given below.

II.D.1 Comminution

To produce fine powders three methods were available: (i) Ball milling, (ii) Fluid energy milling and (iii) Rod milling. A comparative study of the three methods of comminution of RE-Co alloys has shown that (35) rod milling gives narrow size distribution and cause less surface damage of particles and uses less milling time to produce a given average particle size. Hence, rod milling was used in this investigation.

10 gms of an annealed alloy piece was crushed to -100 mesh powder with steel mortar and pestle and used as a feed material for rod milling. 200 non-magnetic stainless steel rods, 13 cm long x 0.31 cm dia. were cleaned using dil. HNO_3 distilled water and then with acetone, thoroughly dried and used for rod milling. A steel cylindrical jar of 9 cm dia. was also cleaned in a similar manner. The alloy powder along with the rods were put in the jar and it was filled with 150 ml of Na treated toluene so that all rods when closely packed completely dipped in toluene. The jar was closed with a lid having an 'O' ring seal and a valve. The jar was evacuated and flushed with high purity argon

(IOLAR) twice and finally filled with argon. The powder was rod milled using a milling speed of 80 rpm. After predetermined intervals of time a few mg of material was taken out from the jar into a small glass boat and dried under vacuum in a desiccator.

II.D.2 Magnet Fabrication

Resin bonded magnets were fabricated using the dried up powder samples collected from the milling jar. Epoxy resin and hardner in a definite proportion (resin : hardner = 3 : 1) were weighed separately on a glass slide and mixed thoroughly for making a homogeneous mixture (this resin to hardner ratio was important for ensuring quick setting of the mixture). The allowable variation in this ratio was found to be about $\pm$ 2 pct.. Beyond this limit, setting of the mixture was improper. Alloy powder was weighed and mixed with the homogeneous mixture of resin and hardner (Powder: (R+H) = 7:3) thoroughly with a piece of stiff metal wire to form a paste of proper consistency. This homogeneous paste was filled into a small glass ampule of ~3 mm dia. and ~7.5 mm length. About 5 mts. time was required to fill the ampule and transfer it into the magnetic field. The filled ampule was aligned in a 5 KOe magnetic field of an electromagnet for 15 mts., the closed end of the ampule was kept in contact with one of the pole pieces of the electromagnet. Ideally the sample should be kept in the magnetic field as long as possible, at least till it hardens to a point when no further orientation of the magnetic particle is possible. For safety of the small magnet,

however it was not possible to keep the sample in the 5 KOe magnetic field for a longer period than 15 mts. During this period there was considerable stiffness produced in the paste filled in the glass ampule. After 15 mts. in the magnetic field the ampule was removed from the magnet and allowed to cure for 24 hrs. in a desiccator. Just before the magnetic measurements were carried out on these samples, their weight was determined. This was required to compute the weight of the sample that got into the ampule, which inturn was required to express the saturation magnetisation and remanance in emu/gm.

CHAPTER III

RESULTS

The resulting of the present investigation can be summarised broadly into two parts: (i) phase equilibria study, (ii) magnetic characterisation.

III.A Phase Equilibria

RE-Co-Fe-Cu-Zr system has been investigated in the composition range of 5.25 to 17.25 at. pct. RE, 56 to 76 at. pct. Co and 10.75 to 18.75 at. pct. Fe, keeping Cu and Zr contents fixed at 8 at. pct. and 2 at. pct. respectively. Here RE is the total Rare-Earth content in cerium rich Indian Mischmetal (MM). Twenty three alloys were studied with an interval of about 2 at. pct. in composition. Alloy compositions used are shown in Fig.III.1 and tabulated in Table III.1.

The phase analysis of 1100°C annealed alloys was carried out using metallography and microhardness measurement techniques, x-ray diffraction analysis and thermomagnetic analysis (TMA). These analysed results are also shown in Table III.1. Results of metallography, TMA, x-ray diffraction, microhardness techniques have been used to attempt identification of phases present and to locate phase boundaries.

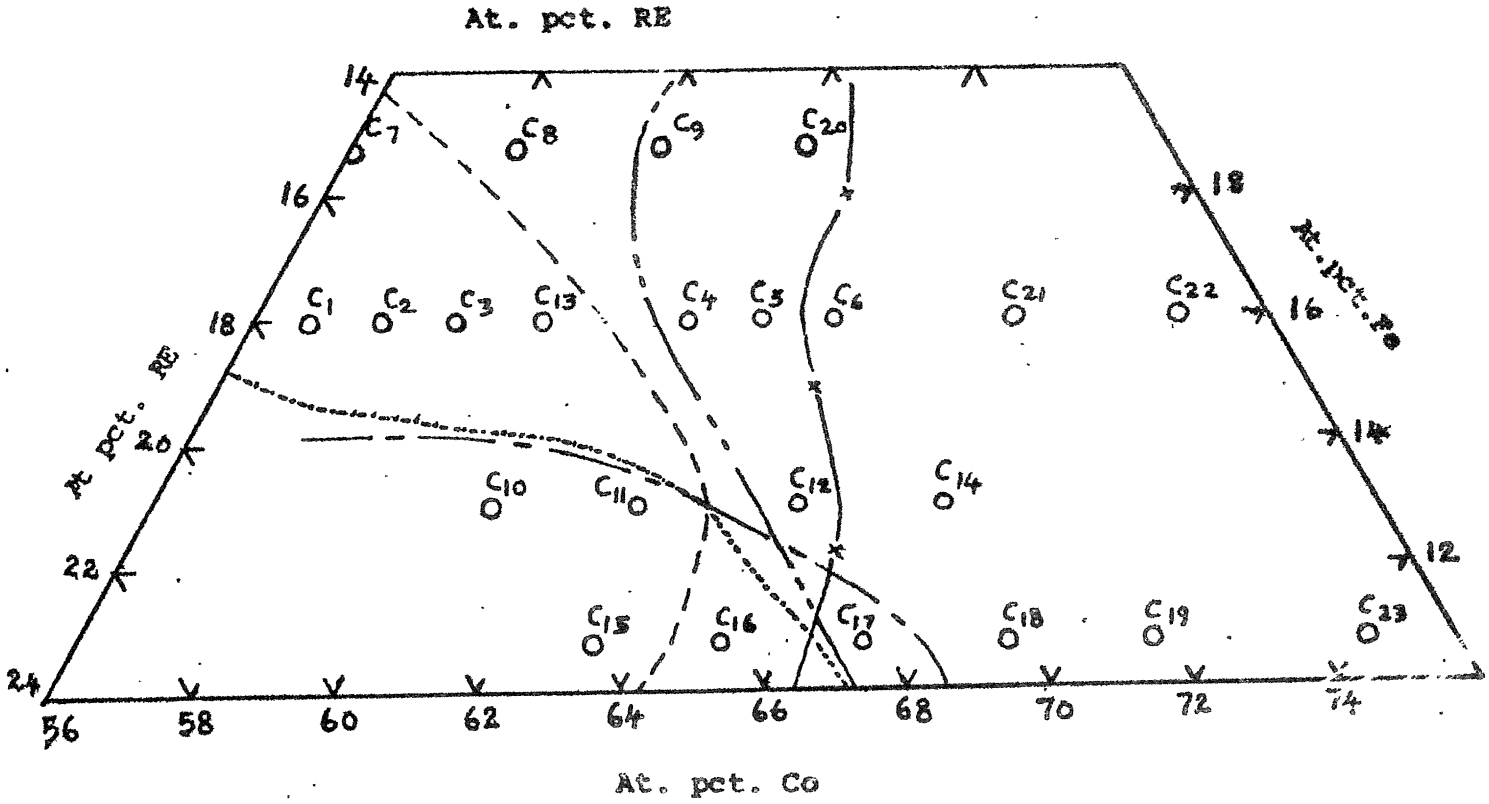

Fig.III.1 Zones of different major phases at 1100°C in RE-Co-Fe-Cu-Zr system.

Notations: L' represents liquid; ..... zone of U;

——— - - ——— zone of Y; - - - - - - zone of U'

——x—— extended zone of L'; ——— - —— zone of N

Table III.1 : Phase Analysis of 1100°C Annealed RE-Co-Fe-Cu-Zr Alloys

Alloy No.	Intended composition, at. pct.					Phase analysis		
	Fe	RE	Co	Cu	Zr	Metallography*	X-ray diffraction analysis	TMA
C_7	18.75	15.25	56	8	2	L' + U + Δ	L' + U	U
C_8	18.75	13	58.25	8	2	U + Δ + Γ'	L' + U	U
C_9	18.75	11	60.25	8	2	U + Γ' + γ	U + γ	U + γ
C_{20}	18.75	9	62.25	8	2	U + Γ' + γ	U + γ	U + γ
C_1	16	17.25	56.75	8	2	L' + U + Δ	L' + U	U
C_2	16	16.25	57.75	8	2	L' + U + Δ	L' + U	U
C_3	16	15.25	58.75	8	2	L' + U + Δ	L' + U	U
C_{13}	16	14	60	8	2	L' + U + Δ	L' + U	U
C_4	16	12	62	8	2	U + γ + Γ'	U + γ	U + γ
C_5	16	11	63	8	2	U + γ + Γ'	U + γ	U + γ
C_6	16	10	64	8	2	U + γ + Γ'	U + γ	U + γ

Continued....

Table III (Continued):

Alloy No.	Intended composition, at. pct,					Phase analysis		
	Fe	RE	Co	Cu	Zr	Metallography*	X-ray diffraction analysis	TMA
C_{21}	16	7.5	66.5	8	2	U + γ + Γ	U + γ	U + γ
C_{22}	16	5.25	68.75	8	2	U + γ + Γ	U + γ	U + γ
C_{10}	13	16.25	60.75	8	2	L' + N + Δ	L' + N	N
C_{11}	13	14.25	62.75	8	2	L' + N + Δ	L' + N	N + U
C_{12}	13	12	65	8	2	U + Γ' + Δ	U + γ	U + γ
C_{14}	13	10	67	8	2	U + γ + Γ	U + γ	U + γ
C_{15}	10.75	16	63.25	8	2	L' + N + Δ	L' + N	L' + N
C_{16}	10.75	14.25	65	8	2	N + Δ + Γ'	N	N + U
C_{17}	10.75	12.25	67	8	2	N + U + γ	N + U + γ	N + U + γ
C_{18}	10.75	10.25	69	8	2	U + γ	U + γ	U + γ
C_{19}	10.75	8.25	71	8	2	U + + Γ	U + γ	U + γ
C_{23}	10.75	5.25	74	8	2	U + + Γ	U + γ	U + γ

* The metallographic identification is given on the basis of metallographic analysis coupled with x-ray diffraction data.

III.A.1 Metallography and Microhardness Measurements

Since most of the alloys of this system are brittle, especially the hign Rare-Earth (RE) containing alloys, extreme care was taken to avoid chipping off of brittle phases during rough polishing. As the high Rare-Earth side alloys are very reactive they needed dilute etchant ($< 2\%$ HNO_3 solution). With increasing Co content of alloys the solution strength had to be increased upto 6% HNO_3. The microstructures of various representative alloys are shown in Fig.III.2a through j.

All the high RE containing alloys showed the presence of a liquid at 1100°C and a small amount of a bright phase particles of geometric shape. The bright phase particles disappeared below 12 at.pot.RE.A phase existing in the high Co containing alloys was found to increase in amount with increase in Co content. This phase appears to be relatively soft compared to the other phases as could be seen from the rate of disappearance of scratch lines from the particles and the matrix phases.

In order to differentiate between phases, microhardness measurement of different observed phases in alloy was carried out. Alloys chosen for microhardness measurement were such that big enough single particles of phases were present in them, so that representative microhardness values were obtained as an average of 10 to 20 measurements on each specimen. Since the measured values of microhardness varied somewhat from alloy to alloy an average value of microhardness for a given phase was computed using all the microhardness data for that phase. The microhardness

Fig.III.2a-j Microstructures of some of the representative alloys of RE-Co-Fe-Cu-Zr system (1100°C, 2d, bulk sample). (1500 x)

a. Micrograph of alloy C_4 shows 3 phases: matrix-U; white phase-γ ; gray phase with internal structure-Γ'

b. Micrograph of alloy C_6 shows 3 phases: matrix-U; white phase-γ ; gray phase-Γ.

c. Micrograph of alloy C_7 shows 3 phases: matrix-U; second phase with internal structure-L'; white geometric crystals-Δ.

d. Micrograph of alloy C_8 shows 3 phases: matrix-U; gray phase with internal structure-Γ'; white geometric crystals-Δ.

e. Micrograph of alloy C_9 shows 3 phases: matrix-U; white phase-γ ; gray phase-Γ.

f. Micrograph of alloy C_{15} shows 3 phases: matrix-N; second phase with internal structure-L'; white geometric crystals-Δ.

g. Micrograph of alloy C_{16} shows 2 phases: matrix-N; white geometric crystals-Δ.

h. Micrograph of alloy C_{17} shows 3 phases: matrix-U; gray phase-N; white geometric crystals-Δ.

i. Micrograph of alloy C_{18} shows 2 phases: matrix-U; second phase-γ.

j. Micrograph of alloy C_{23} shows 3 phases: matrix-γ ; second phase-U; small gray regions-Γ.

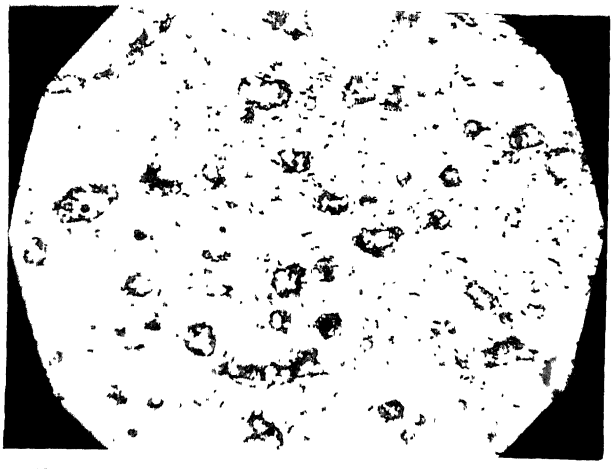

(a)

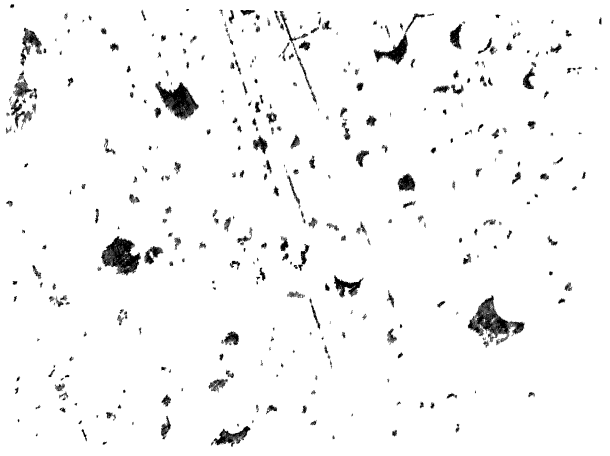

(b)

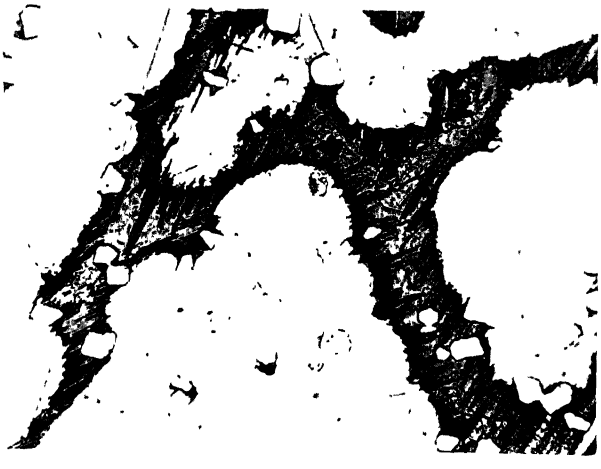

(c)

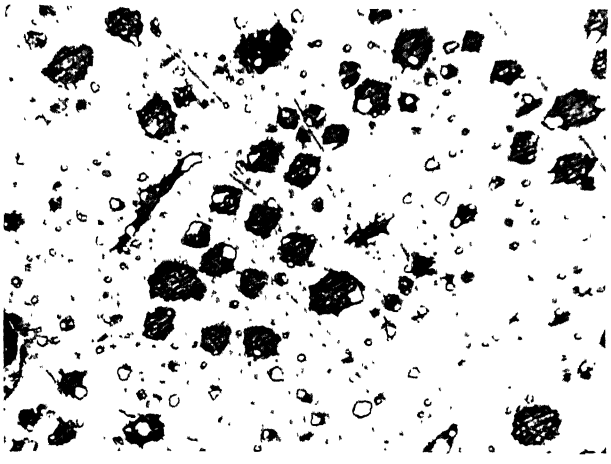

(d)

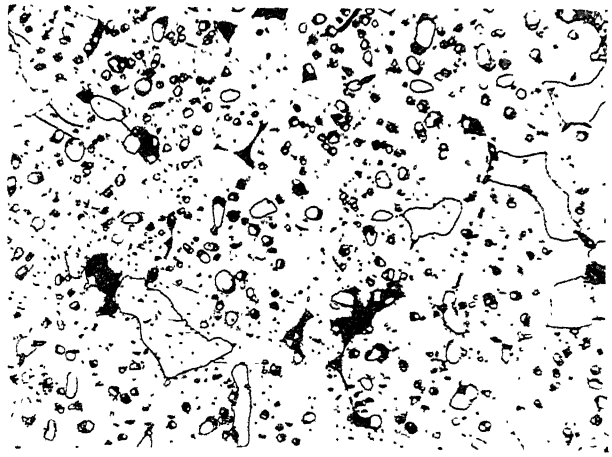

(e)

(f)

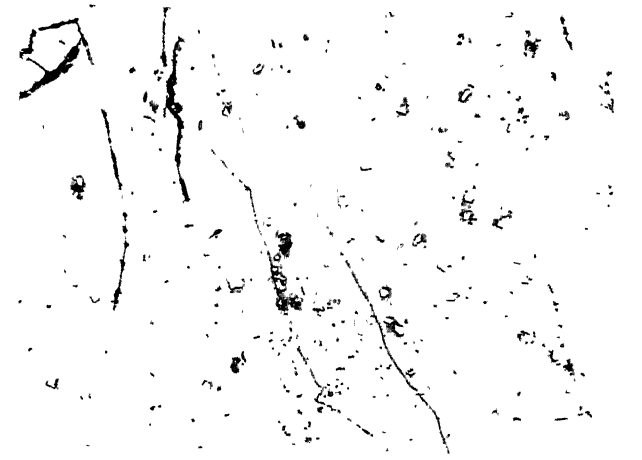

(g)

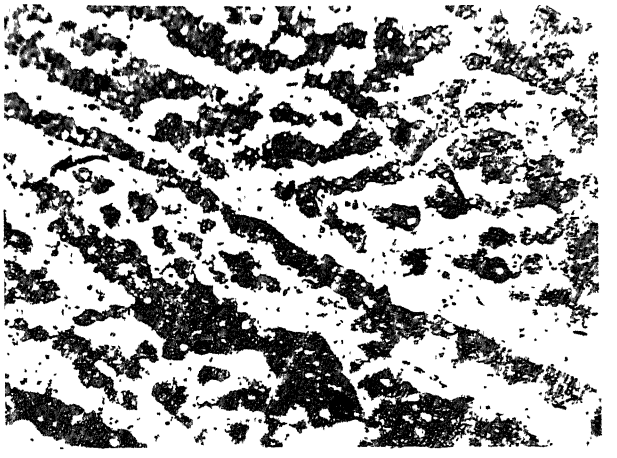

(h)

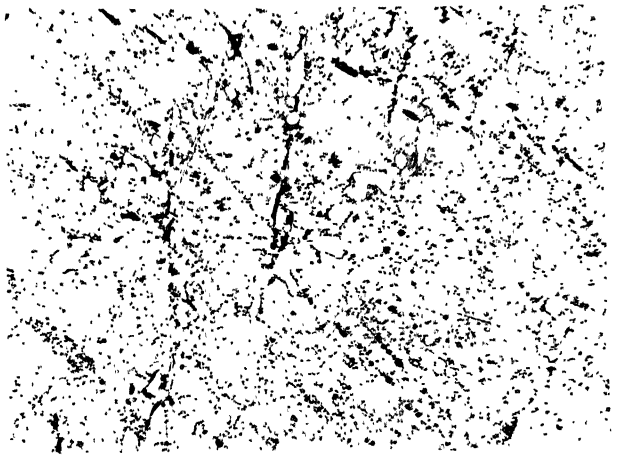

(i)

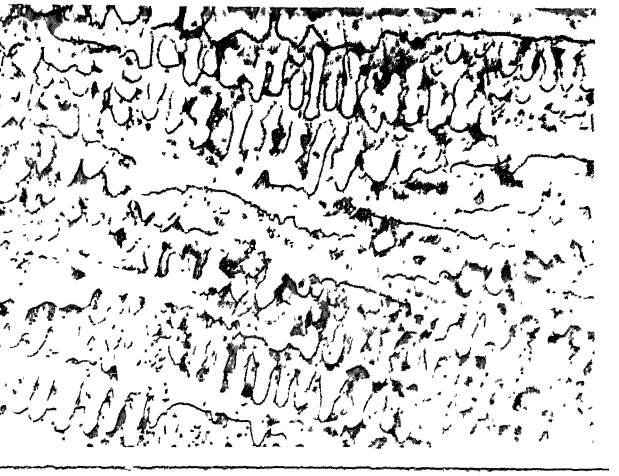

(j)

values of the phases are shown in Table III.2. As may be seen from the data of Table III.1 and Table III.2, the high Co alloys contain a soft phase which is possibly one of the terminal solid solution phases. No clear difference between the matrix phase of various alloys could be established through the micro-hardness measurement.

III.A.2 X-ray Diffraction Analysis

X-ray diffraction patterns of the intermediate phases present in this system are complex and somewhat similar to each other as well as they have their major diffraction lines lying in the same 2θ angular range. So identification of phases in multiphase alloys is quite difficult . Long wavelength radiation ($\lambda_{Cr\ K_\alpha} = 2.2909\ A^\circ$) and slow scanning speeds ($\sim 1.2^\circ$ and in some cases 0.6° per minute) were used for better resolution. By using graphite monochrometer, the diffracted beam was made monochromatic to give only α-radiation diffraction lines and it practically removed all scattered radiations which give rise to background. Inspite of this it was not always possible to have clear resolution of the superimposed major peaks. Phase analysis done by using this technique is presented in Table III.1.

Identification of phases in different alloys was done by comparison of diffraction patterns. The complexity of analysis increased not only because of insufficient resolution but due to (i) the presence of the liquid phase in all the high RE containing alloys and (ii) stress induced structural transformation (fcc → bcc)

Table III.2 : Microhardness Values of Some of the Phases Present in RE-Co-Fe-Cu-Zr System

S.No.	Phase	Microhardness*, vh
1	Matrix	1330
2	Δ	2100
3	γ	320
4	Γ	550

*Microhardness values indicated above are the average values of hardness measured on several alloys.

in high Co containing alloys. The 1100°C annealed alloys were quenched to retain the characteristics of the phases in equilibrium. This gave rise to, nonequilibrium phases arising out of the rapidly solidified liquid phase. With careful analysis, however, it was possible to identify a few diffraction lines arising out of the solidified liquid. Stress induced structural transformation is discussed in a later chapter. For proper phase analysis by x-ray diffraction techniques the high Co containing alloy powders were annealed at 1100°C and water quenched.

Comparison of the diffracted patterns with each other and with the standard patterns of phases existing in the RE-Co-Fe system indicated that (i) the phases existing in the RE-Co-Fe-Cu-Zr alloys are different from that of the RE-Co-Fe system and

(ii) at 1100°C there exists three identifiable phases in the composition region investigated. The alloys C_{17}, C_{18}, C_{19}, which seemed metallographically equivalent to each other, (essentially two phase alloys) showed the presence of a fcc phase (γ) and the other phase (the matrix phase) a new phase designated here as U. The diffraction patterns of the alloys C_{16}, C_{17}, C_{18} clearly showed the presence of two different phases the U phase and another new phase designated here as N (Figures III.3a and 3b).

An attempt was made to index the diffraction patterns of the two newly discovered phases. For indexing a diffraction pattern and to obtain there from reasonably accurate lattice parameters, a specific calibration procedure was adopted. After proper alignment of the diffractometer, a diffraction pattern of a standard silicon specimen was taken. Using the known lattice parameters of Si (a_o = 5.4301 Å), the 2θ position of each reflection from Si was calculated. The calculated and observed 2θ values were compared to find error in the measured angle $\Delta\theta$. The $\Delta\theta_{corr}$ needed for different θ angular regions was plotted (Figure III.4). For the same diffractometer condition, a diffraction pattern of the specimen to be analysed was taken. The diffraction line peak positions were determined and the correction to θ was applied using Fig. III.4. Corrected values of θ were used for indexing the diffraction pattern.

The ductile phase could be separated from the brittle phase, after sieving the crushed alloy powder through a ~250 mesh

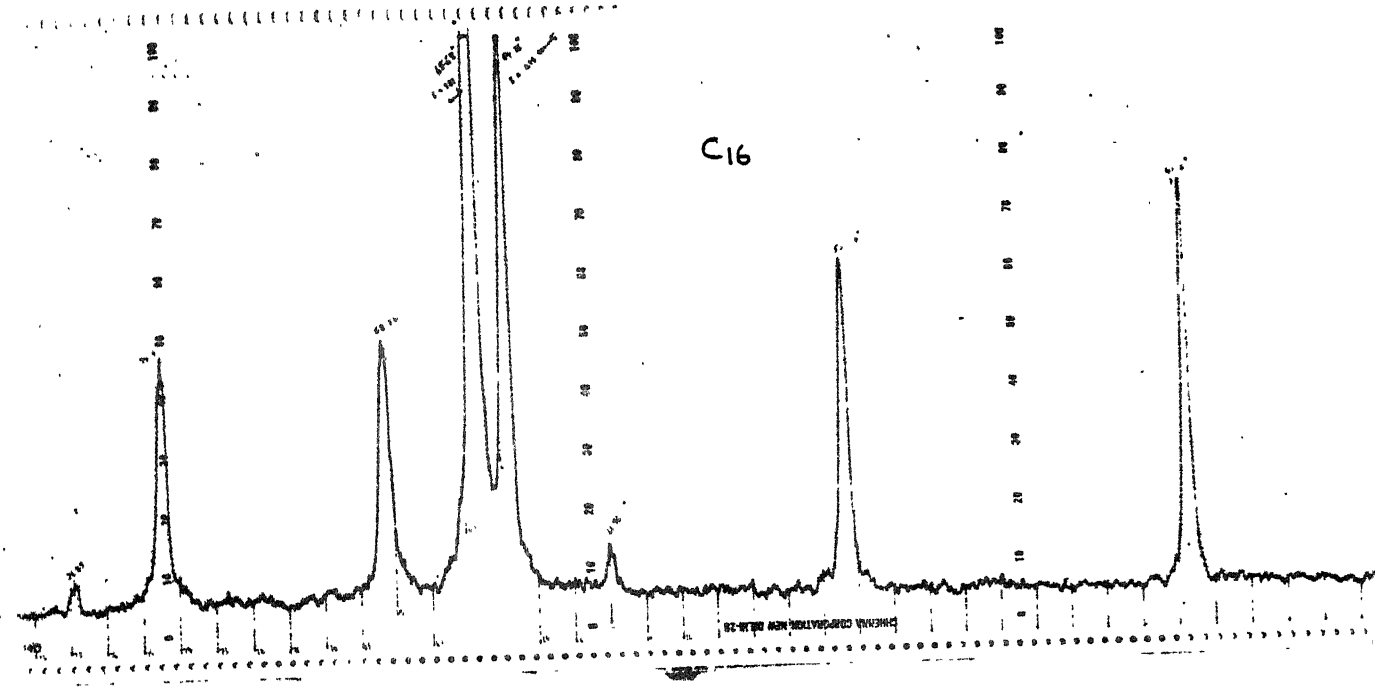

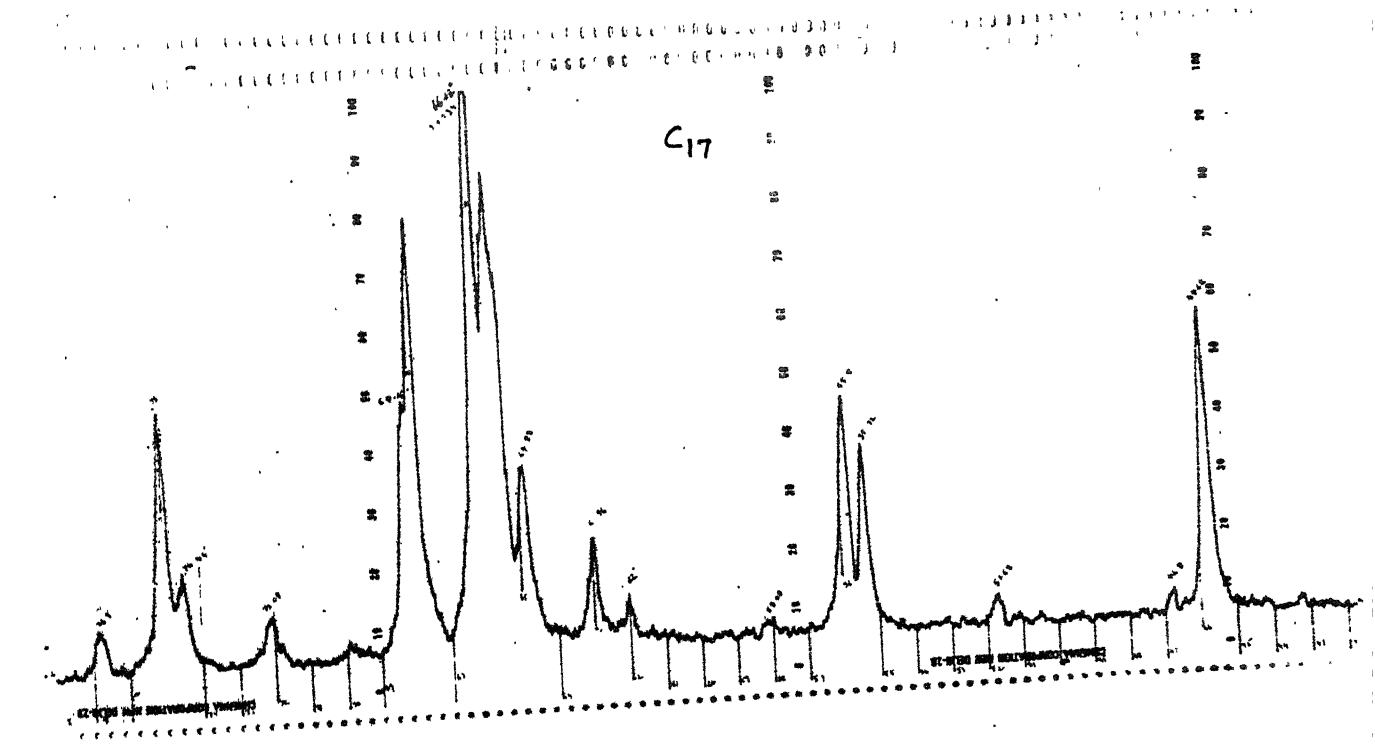

Fig.III.3a : X-ray diffraction pattern of alloys C_{16} and C_{17} annealed at 1100°C for 2 days.

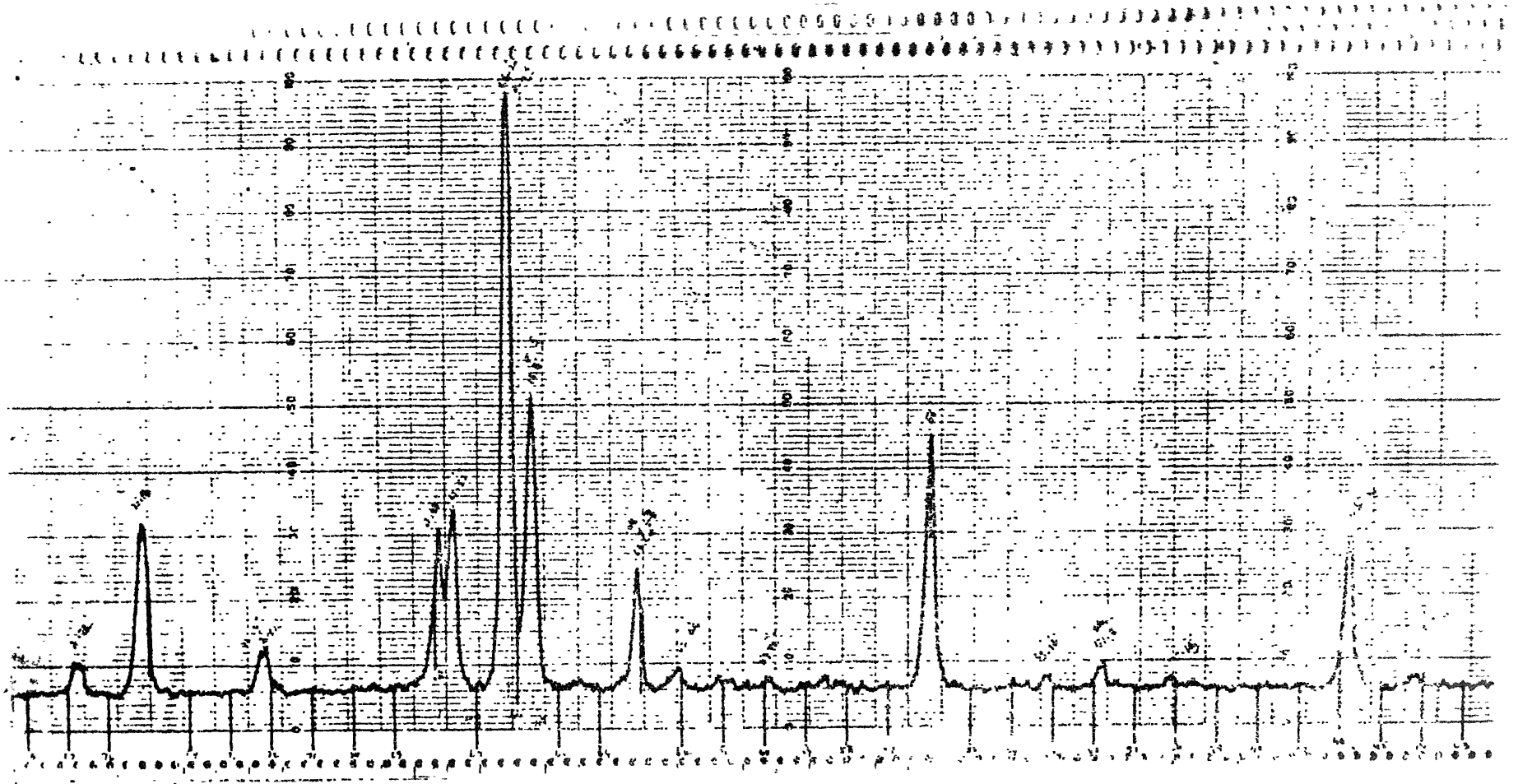

Fig.III.3b : X-ray diffraction pattern of alloy C_{18} annealed at 1100°C for 2 days (stress relieved).

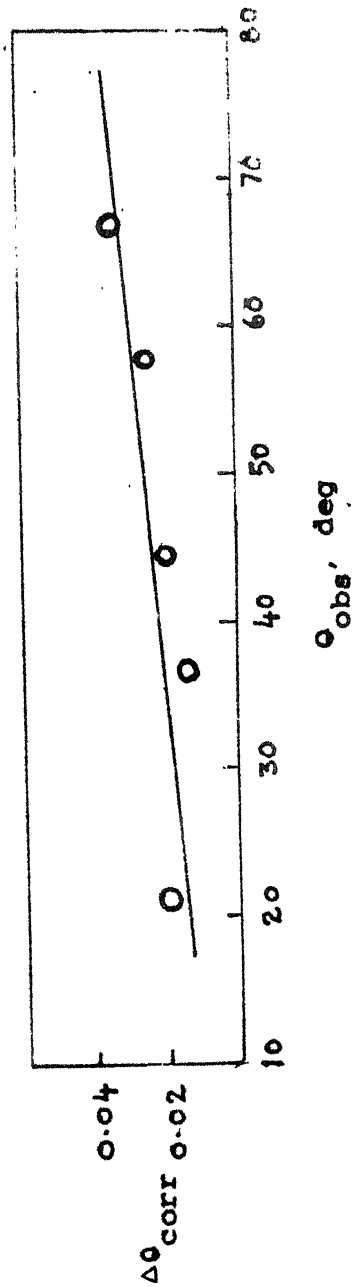

Fig.III.4 Calibration curve for the diffraction angle θ ($\Delta\theta_{corr}$ to be added to the measured θ value).

sieve. The ductile particles, after annealing for 10 minutes at 1100°C (for stress relief), were used for taking a diffraction pattern. This diffraction pattern was also processed in the same manner as described above.

The indexed diffraction pattern of the fcc phase (in alloy C_{14}) is given in Table III.3. The diffraction patterns of the other two phases U and Nare shown in Tables III.4 and III.5. The U phase diffraction pattern could be tentatively indexed on the basis of a hexagonal cell of parameters, $a_o = 5.907$ A°, $c_o = 33.324$ A° and $c_o/a_o = 5.64$. The calculated and observed spacings matched well (Table III.4).

III.A.3 Thermomagnetic Analysis (TMA)

In cases where some or all the phases present are ferromagnetic, it is possible to identify phases and locate phase boundaries by thermomagnetic analysis (TMA). When the more common techniques, metallography and x-ray diffraction do not yield unambiguous results, TMA technique can be used for positive identification of phases. In this case TMA has been helpful in identification of phases. Thermomagnetic analysis of alloys was done using the fabricated permeability apparatus described in Chapter III and Appendix-I. TMA of present alloys has been possible because the magnetic transformation of various phases were found to be reasonably different from each other. Because of the nature of the permeability vs temperature curves, there were often overlap of two transitions and hence great care was

required in interpreting the results.

Table III.3 : Indexed Pattern of γ Phase (Alloy C_{14})
Lattice Parameters, a_o = 3.567 A°

Line No.	Relative Intensity	d_{obs}, A°	hkl	d_{cal}, A°
1	VVS	2.055	111	2.059
2	M	1.781	200	1.783
3	M^+	1.261	220	1.261*

*Line chosen for lattice parameter calculation.
Relative intensity scale: VVS = Very very strong; M = Medium.

TMA results of all investigated alloys are shown in Figs.III.5a to III.5d. In order to know the characteristic features of the permeability vs. temperature trace, a pure Ni sample (99.9% pure Ni powder) was used (Fig. III.5a). In discussing the nature of the permeability vs temperature curve, we consider cooling of the specimen from the higher temperature. In the paramagnetic state the permeability vs temperature trace is parallel to the temperature axis. As the temperature crosses the Curie point, magnetic permeability of the material rises very rapidly. Thus the appearance of the negative slope in the permeability vs temperature trace (during cooling of the specimen) indicates a ferromagnetic transition. If an alloy with more than one phase is cooled from high temperature, the presence of

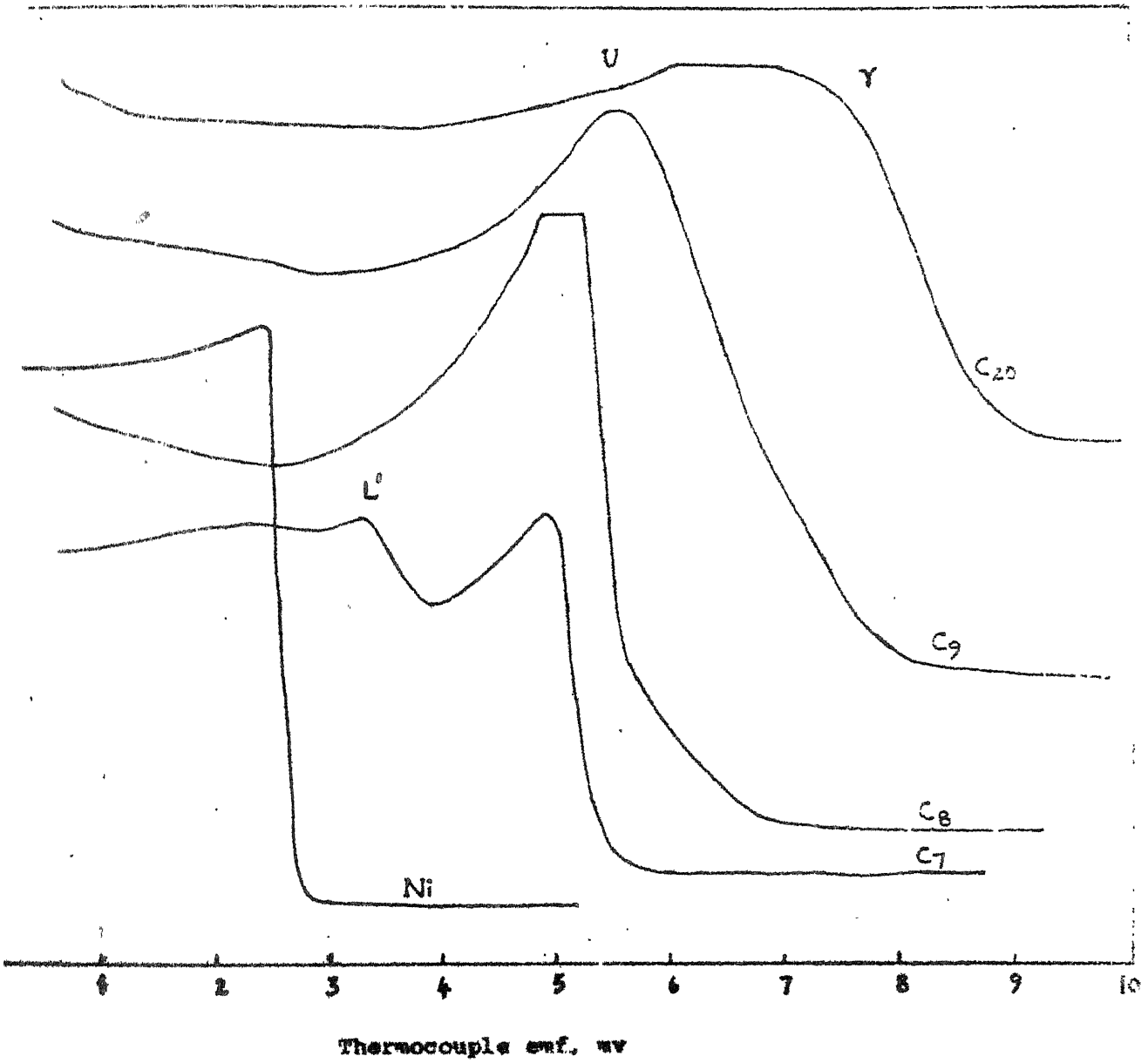

Fig.III.5a Permeability vs temperature traces for RE-Co-Fe-Cu-Zr alloys (C_7, C_8, C_9, C_{20}) containing 18.75 at.pct. Fe and for Ni.

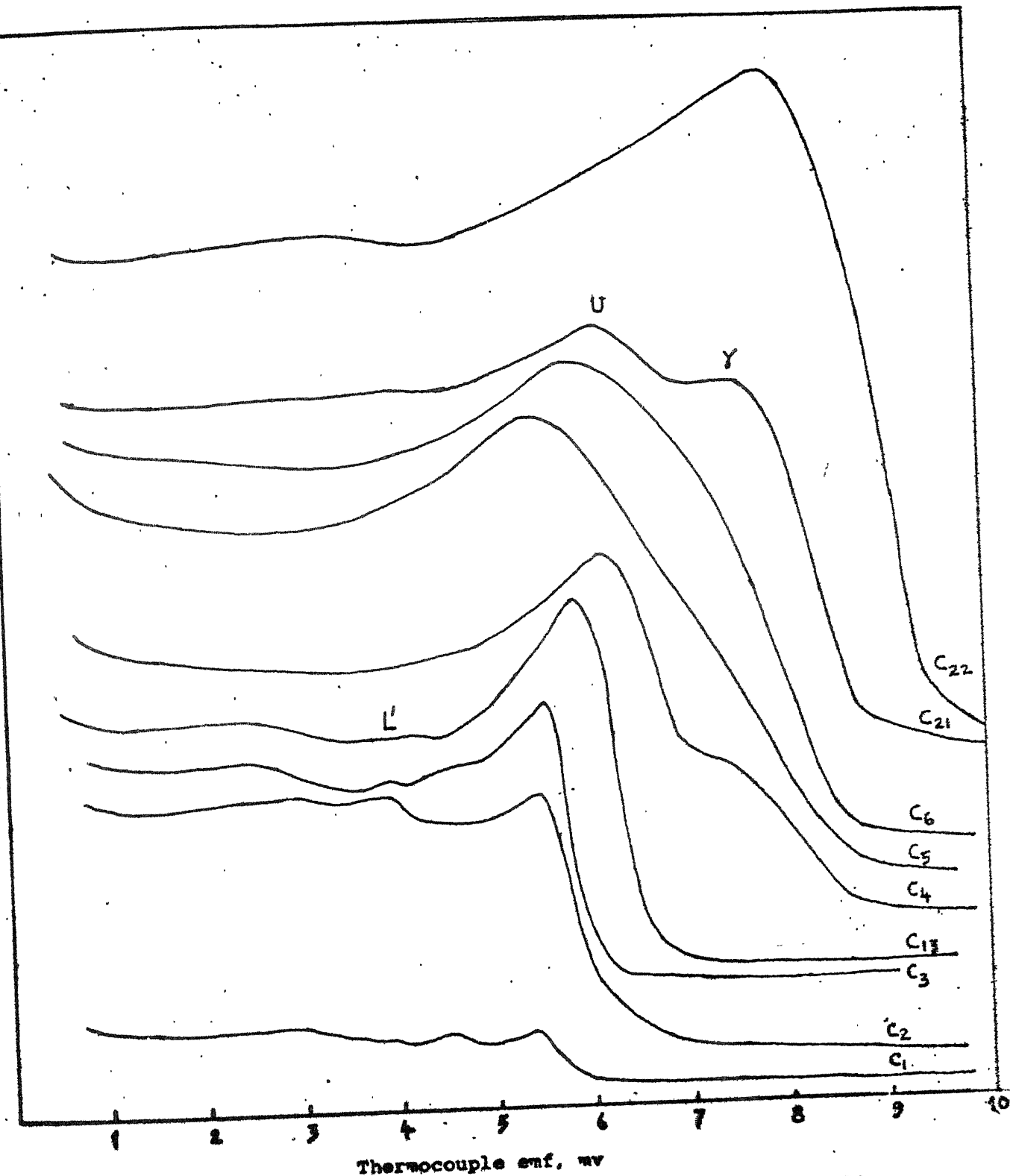

Fig.III.5b Permeability vs temperature traces for RE-Co-Fe-Cu-Zr alloys (C_1, C_2, C_3, C_{13}, C_4, C_5, C_6, C_{21}, C_{22}) containing 16 at.pct.Fe.

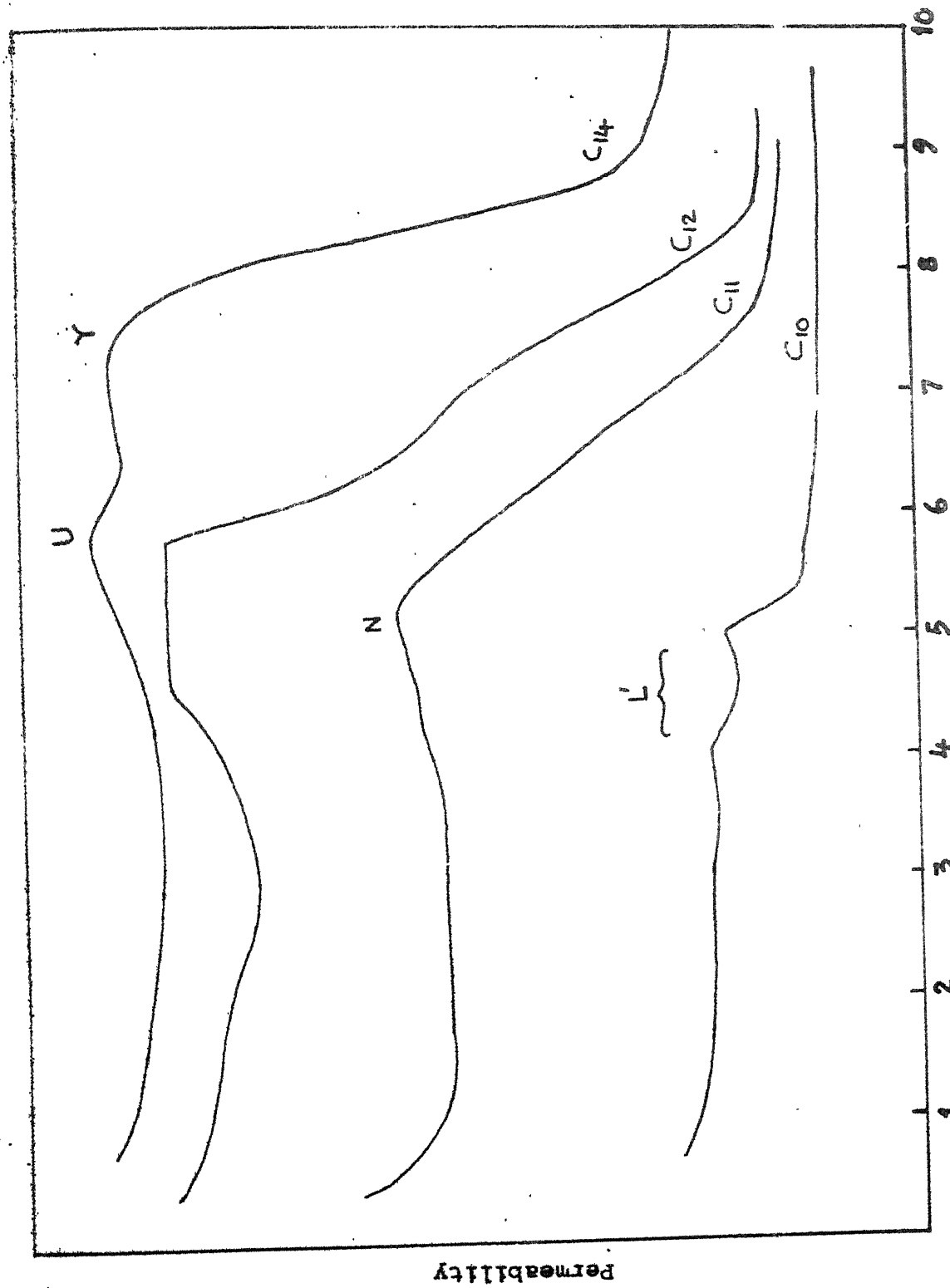

Fig.III.5c Permeability vs temperature traces for RE-Co-Fe-Cu-Zr alloys (C_{10}, C_{11}, C_{12}, C_{14}) containing 13 at. pct. Fe.

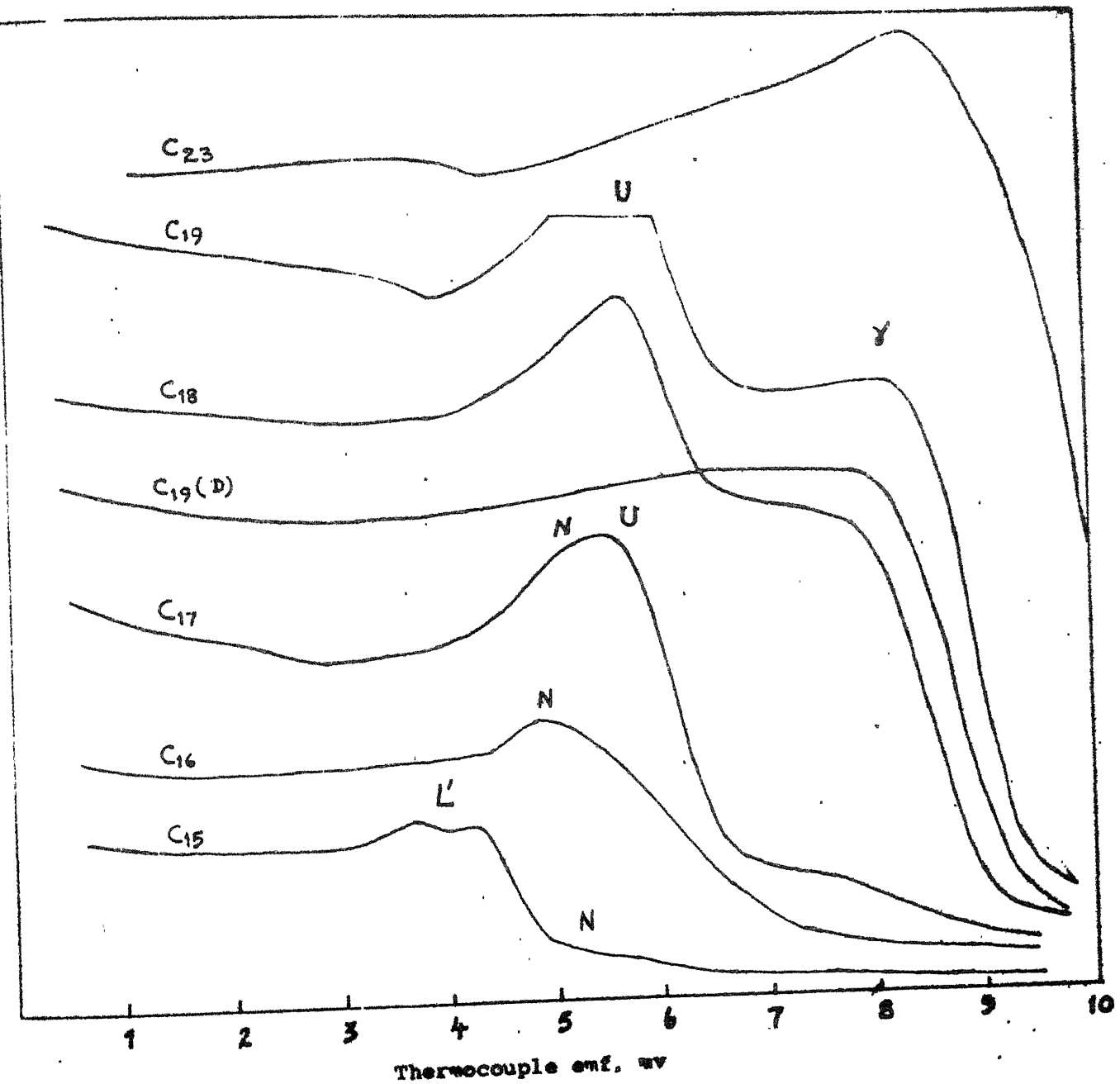

Fig.III.5d Permeability vs temperature traces for RE-Co-Fe-Cu-Zr alloys (C_{15}, C_{16}, C_{17}, C_{18}, C_{19}, C_{23}) containing 10.75 at.pct. Fe.

Table III.4 : X-ray Diffraction Pattern of U Phase in Alloy C_{18}.
Lattice Parameters, a_o = 5.907 A°, c_o = 33.324 A°, c_o/a_o = 5.64.

Line No.	Relative Intensity	d_{obs}, A°	h	k	l	d_{cal}, A°
1	VW	3.340	0	0	10	3.332
2	VVW	3.043	0	0	11	3.029
3	M⁻	2.942	1	1	1	2.942
4	VVW	2.702	1	1	5	2.700
5	VW	2.621	1	1	6	2.608
6	VVW	2.559	2	0	0	2.558
7	M	2.439	1	0	12	2.441
8	VVW	2.293	1	0	13	2.292
9	VVW	2.256	2	0	7	2.253
10	VW	2.219	0	0	15	2.222
11	M⁻	2.189	2	0	8	2.180
12	M	2.113	1	1	11	2.115
13	VVS	2.096	2	0	9	2.105
14	M⁻	2.051	1	0	15	2.038
15	W	1.944	1	1	13	1.936
16	M⁻	1.878	2	0	12	1.881
17	VW*	1.845	0	0	18	1.851
†18	W+	1.787	2	1	7	1.791
19	VVW*	1.645	3	0	5	1.652
20	W	1.571	1	1	18	1.569

Continued...

Table III.4 (Continued):

Line No.	Relative Intensity	d_{obs}, A°	h	k	l	d_{cal}, A°
21	W	1.488	3	0	11	1.486
22	W+	1.472	2	2	2	1.471
23	VW*	1.430	2	2	6	1.427
24	VW	1.410	2	2	7	1.410
25	W+*	1.333	1	2	18	1.337
26	W*	1.300	1	1	23	1.301
27	VVW	1.292	3	0	17	1.287
28	VVW	1.290	1	3	11	1.285
29	W+	1.262	2	1	20	1.262
30	W+	1.261	2	0	23	1.261
31	W	1.235	4	0	7	1.235**
32	W+	1.221	3	0	19	1.222
33	W+	1.220	2	0	24	1.220**
34	M-	1.194	4	0	10	1.194

* Lines are broad
** Lines taken for lattice parameter calculation
† fcc peak is superimposed over this peak

Relative Intensity Scale: VVS = Very very strong; VS = Very strong; S = Strong; M = Medium; W = Weak; VW = Very weak; VVW = Very very weak.

Table III.5 : X-ray Diffraction Pattern of N-Phase in Alloy-C_{16}

Line No.	Relative Intensity	Diffraction angle 2θ, degrees	d_{obs}, A°	Line No.	Relative Intensity	Diffraction angle 2θ, degrees	d_{obs}, A°
1	S	45.6	2.956	14	M⁻	99.36	1.502
2	S	55.28	2.469	15	M	101.64	1.478
3	W	61.96	2.225	16	M⁻	101.80	1.476
4	VS	64.76	2.139	17	W	106.84	1.426
5	VVS	65.68	2.112	18	W	107.00	1.425
6	S	68.24	2.042	19	VVW	108.32	1.413
7	S	74.40	1.895	20	M	116.52	1.347
8	VW	76.88	1.842	21	VW	123.96	1.298
9	VW	89.28	1.630	22	M⁻	135.96	1.236
10	VVW	89.52	1.627	23	M⁻	136.24	1.234
11	W	93.36	1.574	24	M⁻	136.44	1.234
12	W	93.60	1.571	25	S	147.60	1.193
13	M⁻	99.24	1.504	26	M	148.12	1.191

Relative Intensity Scale: VVS = Very very strong; VS = Very strong; S = Strong; M = Medium; W = Weak; VW = Very weak; VVW = Very very weak.

ferromagnetic phases can be detected by the appearance of a change in slope of the permeability vs temperature curve. When the TMA results are analysed in conjunction with the metallographic information obtained for the alloys C_{17}, C_{18}, C_{19}, C_{23} the other characteristic features of the permeability vs temperatures trace can be seen in.X-ray and metallographic technique indicated that alloys C_{23} to C_{17} contain fcc γ phase; the amount of γ phase in alloy C_{17} is very small (only small particles can be seen in Fig.III.2h. The TMA for these alloys (Fig. III.5d) indicate that the sharpness of the rise of permeability decreases as the amount of γ phase decreases and makes it difficult to determine T_c for the phase. Presence of a second phase (U phase) gives rise to a second peak even before the magnetic transformation of the γ phase is completed (C_{18} to C_{23}). Moreover, it may be seen that the fall in permeability of alloy C_{17} (after the permeability peak for U phase is reached) is not as sharp as in the case of C_{18}. This is due to the presence of N phase. The N phase peak becomes more clear in C_{16} in which the U phase peak is less prominent. Finally in alloy C_{15} the U phase peak vanishes and the permeability peak due to the N phase remains together with the permeability peaks due to nonequilibrium phases. T_c is difficult to determine due to the overlap of permeability peaks of different phases. Approximate T_c values for the γ , U and N phases are ~1047°C (from alloy C_{19}), ~832°C (from alloy C_{18}) and ~739°C (from alloy C_{15}), respectively . Because of the overlap of peaks T_c for the phases present in most other alloys was not possible to determine. The shift in the magnetic transition

peak of a particular phase, as we go from high Co to low Co side for an alloy series of a fixed Fe content, suggests that the composition of that phase has changed. Keeping these characteristic features of permeability vs temperature curves in mind, the TMA results of all the rest of the alloys were analysed. The approximate Curie temperatures of these phases are shown in Table III.6.

Table III.6 : Curie Temperatures of Some of the Phases of RE-Co-Fe-Cu-Zr System

Phase	Curie temperature T_c, °C
γ phase (C_{19})	~1047
U phase (C_{18})	~ 832
N phase (C_{15})	~ 739

III.B Magnetic Characterisation of Investigated Alloys

III.B.1 Effect of Heat Treatment on $_iH_c$ in

Around Sm:Tr. metal ratio of 1:7, Sm-Co-Fe-Cu-Zr alloys show magnetic hardenability on low temperature heat treatment. In order to find out which of the investigated alloy will be suitable for detailed magnet fabrication study, bulk specimens of a few alloys (C_4, C_8, C_9, C_{11}, C_{12}, C_{13}, C_{17}) were chosen for low temperature heat treatment. 1100°C annealed piece of each

chosen alloy was aged at 675°C for different lengths of time and the $_iH_c$ was measured after each duration of heat treatment. The results of this investigation are shown in Fig.III.6. Among all the alloys studied, the alloy C_{11} was found most promising and hence further study was made to find whether any other temperature will be more suitable to enhance the $_iH_c$. Aging temperature of 650°C and 620°C were chosen. The results are shown in Fig.III.7.

The result of 650°C aging treatment has not been shown here because of some inconsistency in data which arose due to power failure. There was not much improvement in coercivity compared to 675°C heat treatment. Variation of $_iH_c$ with aging time for alloy C_{11} at 620°C is shown in Fig.III.7. The microstructure of 466 hr aged alloy C_{11} is shown in Fig.III.8b along with non aged microstructure in Fig.III.8a.

III.B.2 Effect of Particle Size on $_iH_c$

Magnetisation of a fabricated magnet depends on the particle size and particle size distribution of the material used in magnet fabrication and the two parameters depend quite significantly on the milling method and the milling time. Rod milling has been found to give close size distribution and taking less grinding time for producing a given average particle size (35). Hence, rod milling was used in this investigation. To find the critical milling time for obtaining best $_iH_c$, annealed alloy C_{11} was ground for different lengths of time. Resin bonded samples were

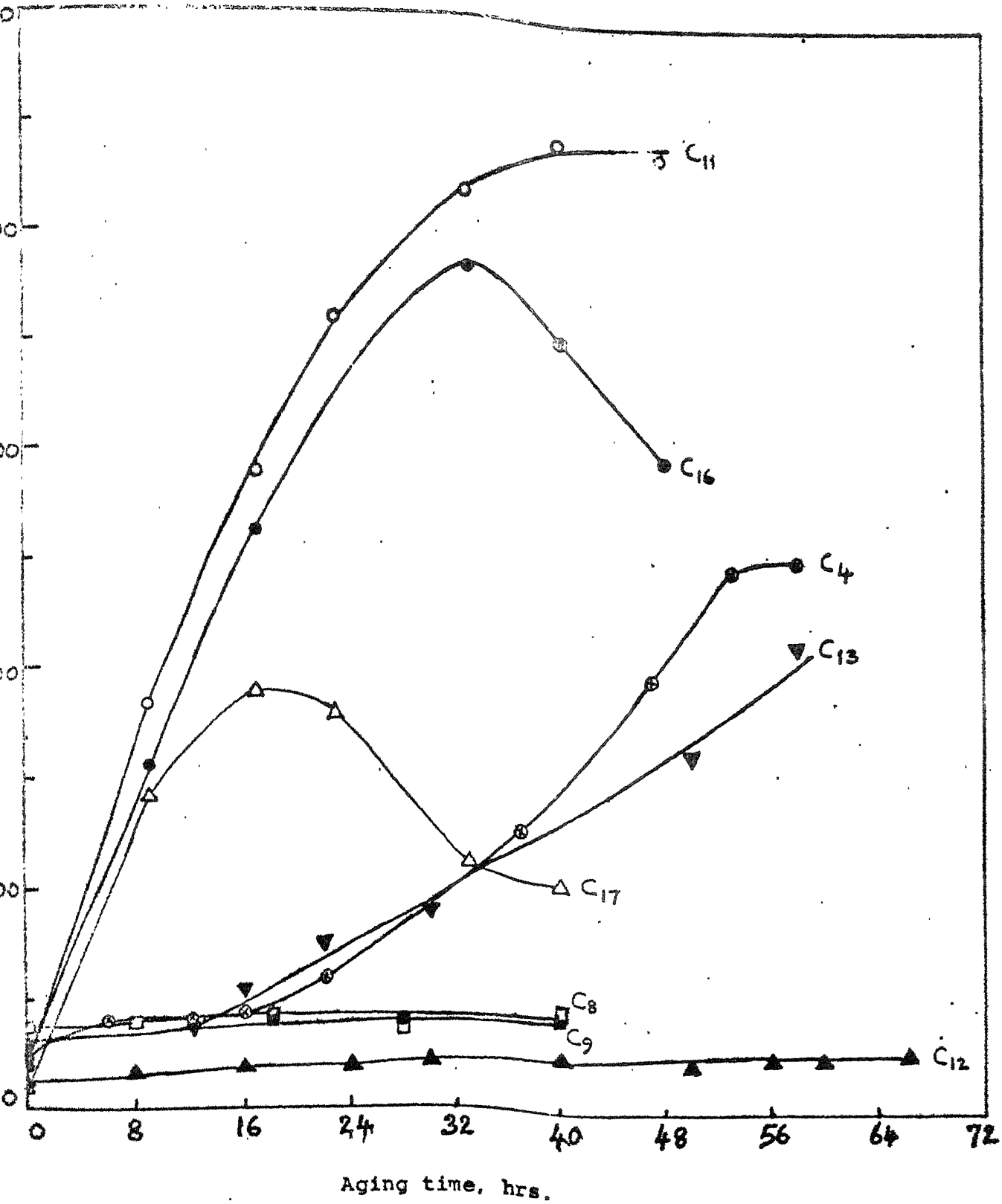

Fig.III.6. Intrinsic coercivity vs aging time for alloys (C_4, C_8, C_9, C_{11}, C_{12}, C_{13}, C_{16}, C_{17}).

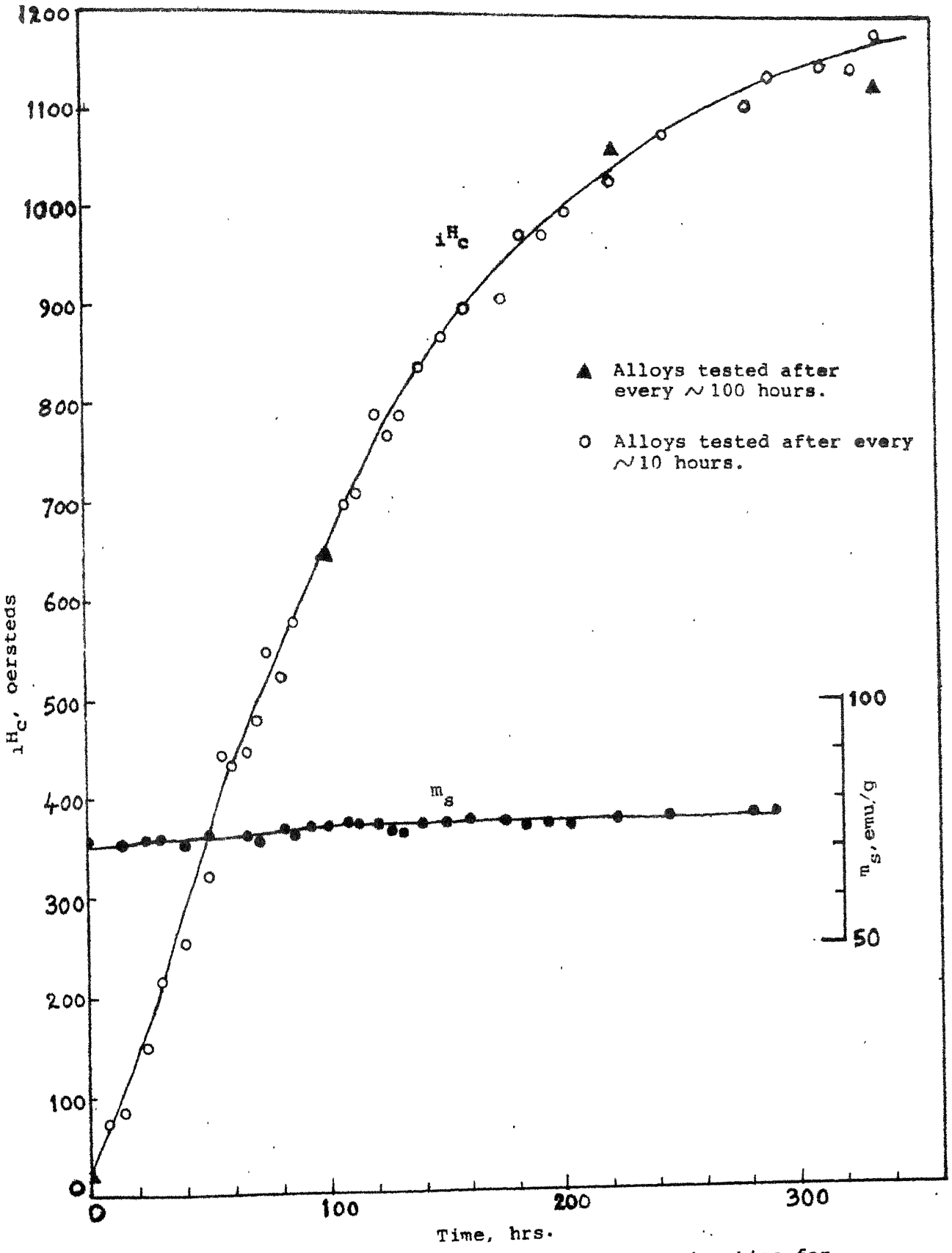

Fig.III.7 Variation of magnetic properties vs aging time for alloy C_{11}.

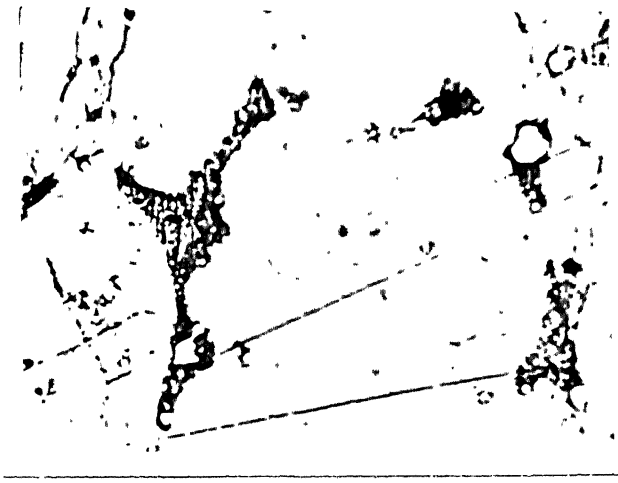

(a)

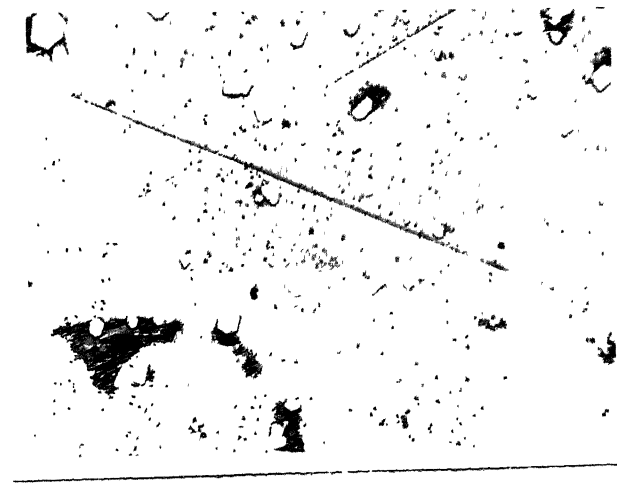

(b)

Fig. III.8 : Microstructures of alloy C_{11} (a) non-aged and (b) aged conditions: matrix - N; gray phase with internal structure - L'; white geometric crystals- Δ. (1500 x)

were measured as a function of milling time and are shown in Fig.III.9 and Table III.7.

Table III.7 : Magnetic Properties of Resin Bonded Samples

Milling time (hrs)	$_iH_c$, Oe	M_s (emu/gram)	M_r/M_s
2	313	81.01	0.457
2½	340	77.27	0.573
3	-	-	-
3½	390	-	-
4	400	75.76	0.500
5	424	80.29	0.571
6	460	74.88	0.548

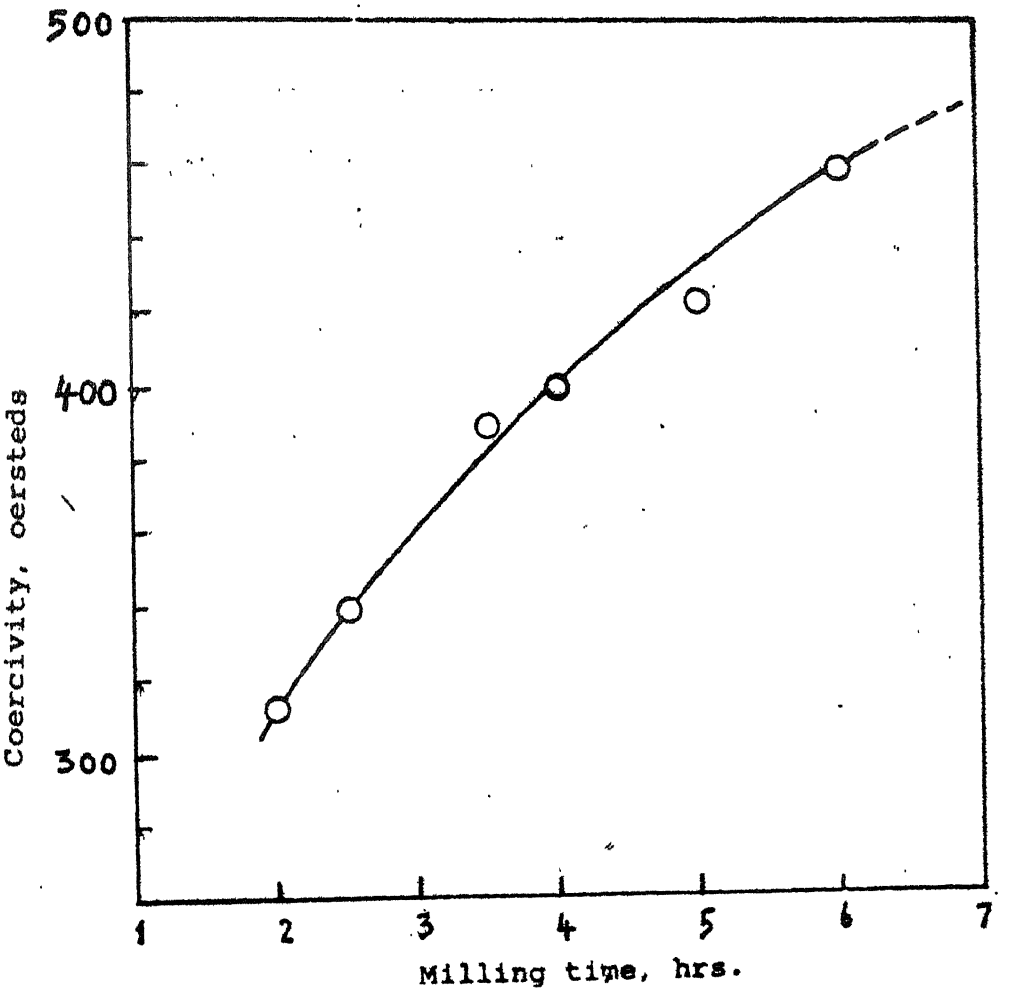

Fig.III.9 Intrinsic coercivity vs milling time for alloy C_{11}.

CHAPTER IV

DISCUSSION

The present investigation essentially has two major thrusts: (i) to understand the phase equilibria in the complex alloy system RE-Co-Fe-Cu-Zr where RE is a mixture of light rare-earth elements found in Indian mischmetal and (ii) magnetic characterisation and study of process parameters for magnet fabrication. Of these the first aspect has been studied in somewhat more detail in this investigation. In the following sections the results obtained have been discussed.

IV.A Study of Phase Equilibria in RE-Co-Fe-Cu-Zr System

IV.A.1 Phase Analysis in the Investigated Region of the RE-Co-Fe-Cu-Zr System

Phase equilibria in RE-Co-Fe-Cu-Zr system has been determined using Mischmetal (MM). Since Indian MM contains some amount of Fe, to represent phase equilibria all the Fe that is present in MM (12 wt. pct.) and that is added intentionally have been considered together. Thus MM-Co-Fe-Cu-Zr system has been represented here as RE-Co-Fe-Cu-Zr system in which RE represents the total rare-earth content of MM. Since the individual rare-earth elements, La, Ce, Pr, Nd are soluble in each other to a large extent, it has been assumed that RE represents a solid solution of rare-earth elements and for representing phase equilibria RE has been considered as a single component.

The phases present in the various alloys have been analysed by metallography, x-ray diffraction and TMA techniques and are shown in Table III.1. Metallography of the alloy C_7 (Fig.III.2c) containing 18.75 at.pct. Fe showed the presence of a liquid phase at 1100°C. Due to non-equilibrium cooling of the liquid, a non-equilibrium structure, designated here as L', has been produced within the liquid phase. L' produced a few characteristic diffraction lines shown in Fig.IV.1 and an internal structure within the solidified liquid can be seen in the microstructure Fig.III.2c. This liquid phase is verified by annealing a 1100°C annealed alloy piece at 1150°C for half an hour and water quenched to retain the phases present. On microstructural examination, the liquid phase was found to increase in amount compared to that at 1100°C as can be seen from Fig.IV.2a and b. On macro examination the 1150°C annealed alloy had many pores in it and the corners were rounded off indicating melting of the alloy. The matrix phase could be identified as the U-phase. Besides these features, the microstructure of alloy C_7 also showed some bright geometric shape particles. Since the amount of this phase, designated here as the Δ phase, in the alloy C_7 is rather small no diffraction lines could be identified as due to the Δ phase. The Δ phase disappeared when RE content was less than 13 at.pct. The other alloys containing 18.75 at.pct. Fe, i.e., C_8, C_9 and C_{20}, showed the matrix phase to be U-phase. A gray phase, Γ', showing some internal structure could be seen in the microstructure alloy C_8 (Fig. III.2d). Even though the morphology

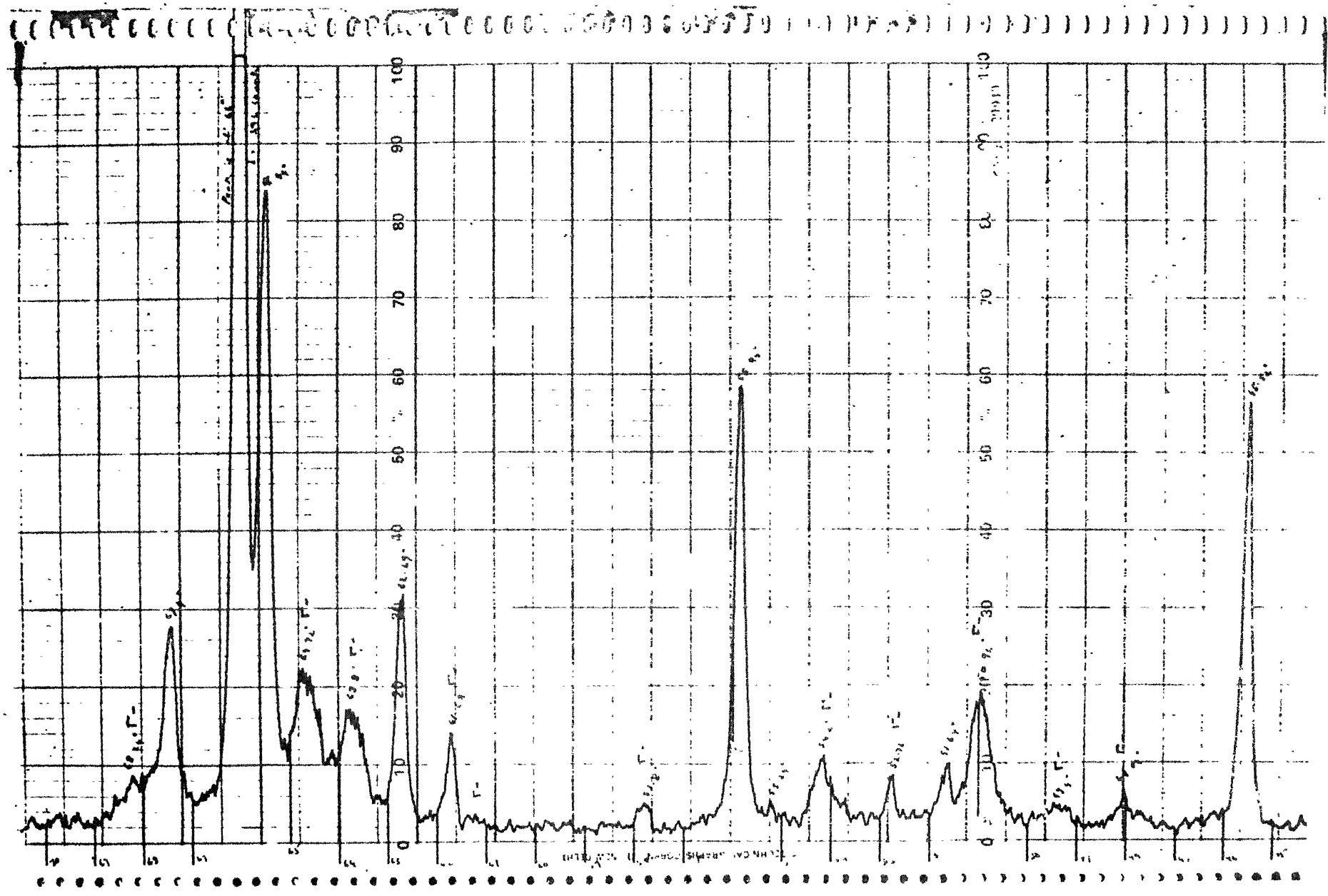

Fig.IV.1 : X-ray diffraction pattern for L'-phase lines in

(a)

(b)

Fig.IV.2 : Microstructures of alloy C_1 at (a) 1100°C and (b) 1150°C show 3 phases : matrix-U; second phase with internal structure-L'; white geometric crystals- Δ. (1500 ×)

of the Γ' phase was found different from the liquid phase, the microstructure of alloy C_9 (Fig.III.2e) shows in some places the characteristic angular feature of a liquid phase entrapped between grains. Since the amount of Γ' phase is not very large and that the characteristic diffraction lines due to L' are of low intensity, it was not possible to identify through x-ray diffraction patterns whether Γ' is in reality L'.

The alloys containing 16 at. pct. Fe and $\geq$ 14 at. pct. RE i.e., alloys C_1, C_2, C_3 and C_{13} were microstructurally same as the alloy C_7, i.e. contained L' + U + Δ. In alloys containing 11 and 12 at. pct. RE (alloys C_4 and C_5) the Γ' phase appeared together with a fcc γ phase. The γ phase could be identified clearly through the permeability traces obtained for these alloys. Since the fcc phase produced in the microstructure very small islands, which also appeared bright under microscope illumination, it was not possible to determine whether these alloys also contained any Δ phase or not. In alloys C_6, C_{21} and C_{22}, containing 16 at. pct. Fe and 5 at. pct. $\leq$ RE $\leq$ 10 at. pct., no Γ' phase was found. Instead a new gray phase, Γ, without showing any internal structure within the gray phase region (Fig.III.3b) was observed. The identified equilibrium phases for these alloys are U + γ + Γ.

The alloys containing 13 at. pct. Fe and 14 to 16 at. pct. RE (C_{10} and C_{11}) and 10.75 at. pct. Fe and 16 at. pct. RE (C_{15}) showed, unlike the alloys containing 16 at. pct. Fe and 18.75 at. pct. Fe alloys and about the same amount of RE, i.e. C_7, C_1 and C_2, the presence of a liquid phase together with Δ and a new phase

designated here as the N phase. Decrease in RE content for the 13 at. pct. Fe alloys caused a change in the phases present; liquid phase vanished and in its place small amount of Γ' phase appeared, the N phase was replaced by U and fcc γ phase appeared. On further decrease in RE content the phases found were U $+\gamma+\Gamma$. Unlike the 13 at. pct. Fe alloys, decrease in RE content of 10.75 at. pct. Fe alloys first produced N + A+ Γ' (C_{16}) then U + N + γ(C_{17}) followed by U + γ (C_{18}) and finally U $+\gamma+\Gamma$(C_{23}).

IV.A.2 Stress Induced Transformation of the γ Phase

Higher Co containing alloys were found relatively more difficult to powder than higher RE containing alloys. This is due to the fact that the higher Co containing alloys contained various proportions of the γ phase. For x-ray diffraction work the alloys were powdered using steel and agate mortors and pestles. The as obtained powder was used for preparing x-ray powder specimens. For brittle alloys, like the ones encountered in the present case, the diffraction patterns are usually sharp and powder does not require annealing for stress relief. The ductile phase diffraction lines become somewhat broad but can be identified easily when present in sufficiently large amount. Since the alloys of the present investigation are very reactive, annealing of alloys in fine powder form causes oxidation and preferential loss of RE component due to oxidation. This is the main reason why annealing of fine powders of RE containing alloys is usually avoided and was not done in the beginning in the present study. This caused considerable difficulties in phase analysis.

During the phase analysis of high Co containing alloys x-ray diffraction pattern not only showed fcc phase but also showed presence of very strong diffraction line due to a bcc phase. The bcc phase lattice parameter was calculated on the basis of (110) reflection to be $a_0 = 2.840$ A°. In Co-Fe system the fcc terminal solid solution of the Co side is followed by a bcc phase if the temperature is $\lesssim 950°C$. The appearance of the bcc diffraction lines in the x-ray diffraction patterns of alloys annealed at 1100°C thus suggested that the addition of RE, Cu and Zr to the Co-Fe system stabilises the bcc phase RE-Co-Fe-Cu-Zr system so that it exists at 1100°C. It was, however noticed that the bcc phase diffraction line intensities did not vary in a systematic manner, as the alloy composition was changed. No trace of any bcc phase in the microstructure also could be detected. Moreover, when the same powder specimen (the ones used for x-ray analysis) was used in the permeability apparatus to determine the magnetic transition of the phases, no extra magnetic transition due to the bcc phase could be found. Since for magnetic transition temperature determination the powder is first heated to a $\sim$1050°C the powder gets annealed. Hence it was thought that the bcc phase may be arising out of stress induced transformation of the fcc γ phase.

To test this the powder of alloy C_{22} was sealed in an evacuated silica capsule and annealed at 1100°C for 10 min. and then water quenched. After stress relief the powder was used to take a x-ray diffraction pattern which showed almost complete elimination of the diffraction line due to the bcc phase and there

was a corresponding increase in the intensities of the fcc phase diffraction lines. To see whether the bcc phase (α) diffraction line again reappears on cold working, the annealed powder was hammered in a steel mortar and pestle for 15 minutes. The x-ray diffraction pattern after this cold work again showed appearance of a sharp bcc phase diffraction line and decrease in intensities of the fcc phase diffraction lines (Fig. IV.3). This test conclusively showed that a stress induced transformation causes generation of the bcc phase from the fcc γ phase. Thus, the bcc phase is not an equilibrium phase at 1100°C.

A similar test was carried out for the alloys C_{16}, C_{17} and C_{18} containing N, N + U and U phases. In this case a change over from N to U structure was observed when the powder specimens of alloy C_{16} and C_{17} were annealed at 1100°C for stress relief. The annealed powder on hammering, however, did not bring back the N phase indicating that the change of structure produced by annealing of powder specimen is not due to stress. Since the alloy containing N and U phases has higher RE content and that there is always a slight oxidation of the RE component of the rare-earth base alloy, the change in structure after powder annealing is due to oxidation and not due to stress. Fig. IV.4 is showing a portion of x-ray diffraction pattern of alloy C_{16} before and after stress relief.

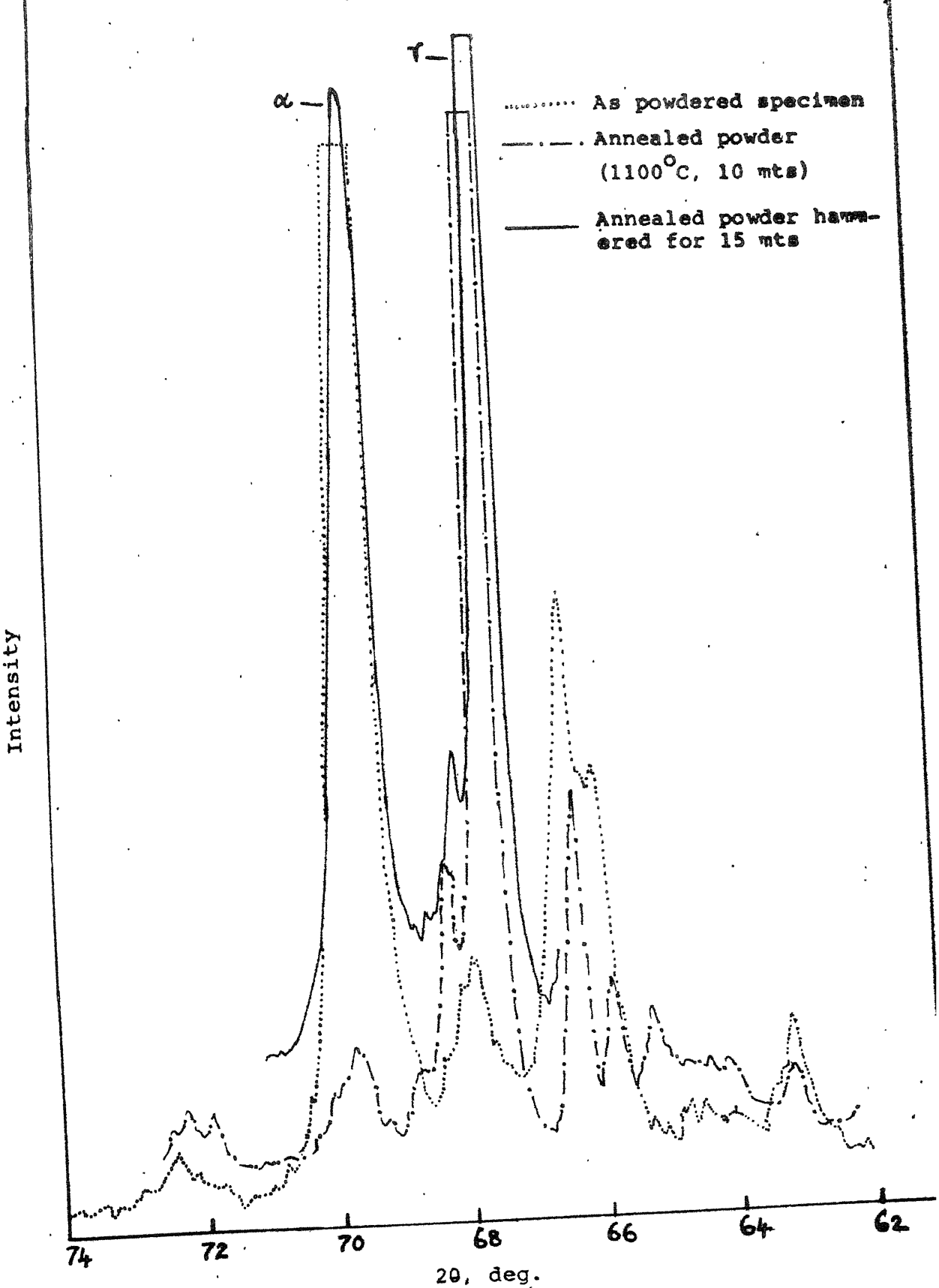

Fig. IV.3 X-ray diffraction patterns showing stress induced γ(fcc) ⟶ α(bcc) transformation in alloy C_{22}.

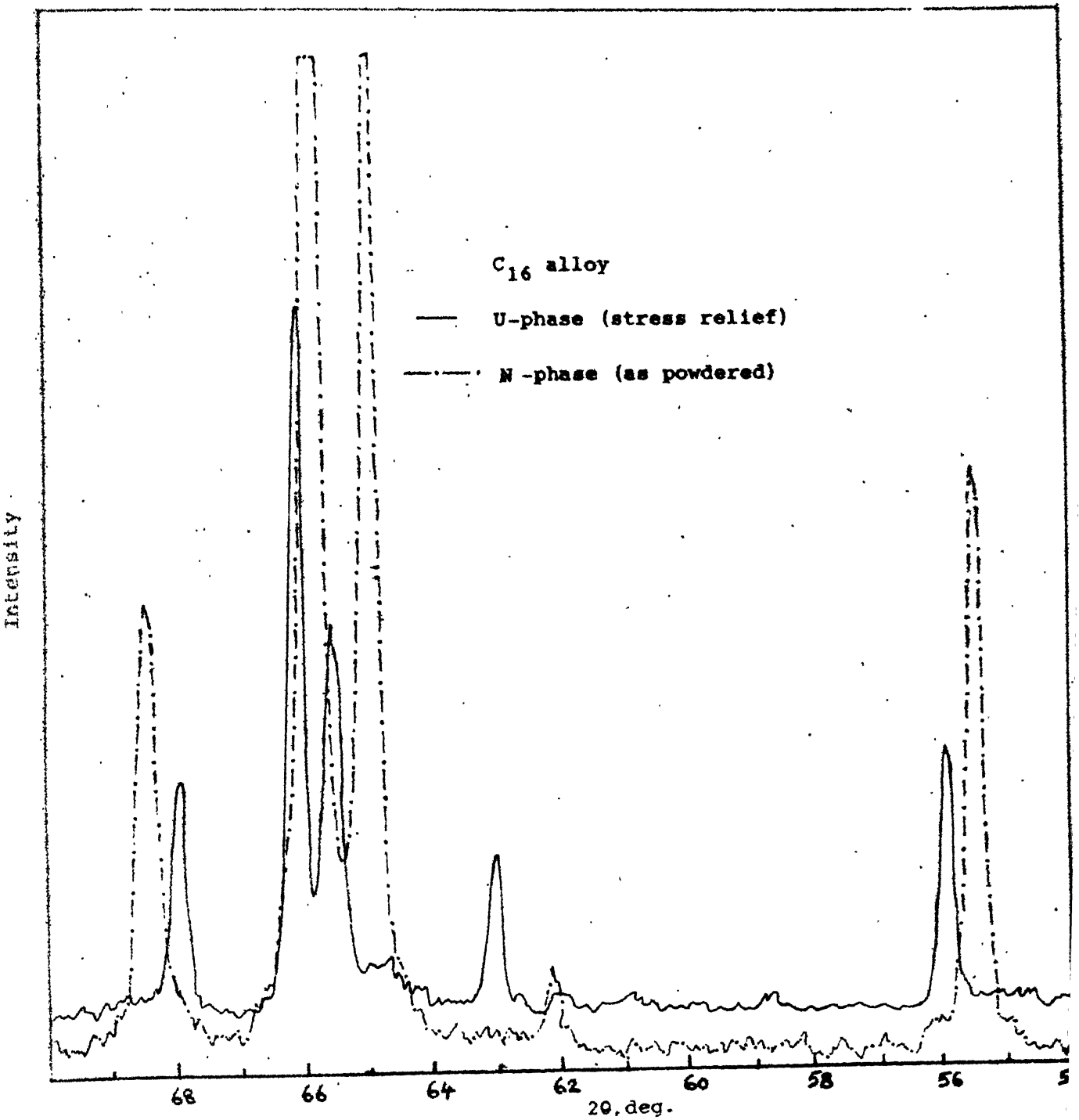

Fig.IV.4 X-ray diffraction pattern of alloy C_{16} in the as powdered (N-phase) and annealed (U-phase) states.

IV.A.3 Phase Equilibria

Through the analysis of alloys it was not possible to determine a true phase equilibria in terms of proper phase boundaries in a 1100°C isothermal section. The reason for this is that the investigation is localised within a reasonably narrow composition region which is important from magnetic property point of view. Hence, this limited investigation does not allow exact location of the L', U, N and γ phase regions. The Fig.III.1, which shows location of all the alloy composition investigated, can be divided into four clear regions representing zones of L', γ, N and U phases. If the L' phase is the same as L', the zone of liquid phase will extend further to the right of the diagram i.e., to lower RE contents. This is also shown in Fig.III.1. At 1100°C Co solid solution phase (fcc) is stable. Hence, the γ phase observed can be identified as the fcc Co solid solution phase. The zones of γ phase and U phase also indicate that the γ phase region must be located towards the bottom right hand corner of the diagram. Since the U phase is found in the zone of γ phase as well as in the higher Fe containing part of the zone of liquid phase it implies that the U phase is a high Fe containing phase located somewhere at the top of the diagram. The liquid phase zone is to the left of the diagram, i.e., at higher RE contents. Since the N phase is not found above 13 at. pct. Fe, the N phase must be located at a lower Fe content than 11 at. pct. Fe towards the left hand side corner of the diagram.

IV.B. Effect of Alloying Elements on the Phase Equilibria of RE-Co-Fe System

As discussed in the last section the RE-Co-Fe alloys containing fixed amounts of Cu and Zr gave entirely different set of phases compared to the RE-Co-Fe alloy system . To find whether this is due to Cu or due to Zr, a cursory study of RE-Co-Fe-Cu system was done using only three alloys $C_1(a)$, $C_6(a)$ and $C_{17}(a)$ having the same RE and Cu contents as that of the Zr containing alloys C_1, C_6 and C_{17}. The alloy compositions used are shown in Table IV.1. Phase analysis for these alloys annealed at 1100°C was done in the same manner as the Zr containing alloys and are shown in Table IV.1. A 2:17 phase was found in all the alloys. The alloy $C_1(a)$ also showed the presence of a liquid phase at 1100°C. The other alloys showed the presence of a fcc phase in addition to the 2:17 phase. The indexed 2:17 phase diffraction pattern is shown in Table IV.2. The microstructure of these alloys are shown in Fig.IV.5a to IV.5c to show some of the characteristic features of these alloys and TMA traces are shown in Fig.IV.6.

Alloy $C_1(a)$, RE : TM = 1 : 4.8 is close to the 1:5 phase region in the ternary RE-Co-Fe (18) phase diagram. Alloys $C_6(a)$, RE : TM = 2:18 and $C_{17}(a)$, RE : TM = 2:14.3 falls in the 2:17 phase region of the ternary system. Velu (21) has reported that even in 1:5 (MM : TM) alloys of MM-Co-Cu system if Cu is present in low contents (below 17 at. pct.) 2:17 phase exists along with 1:5 phase. So RE-Co-Fe-Cu system is showing basically

Fig.IV.5a : Microstructure of alloy C_1(a) shows 2 phases: matrix - 2:17; second phase with internal structure-L'. (1500 x)

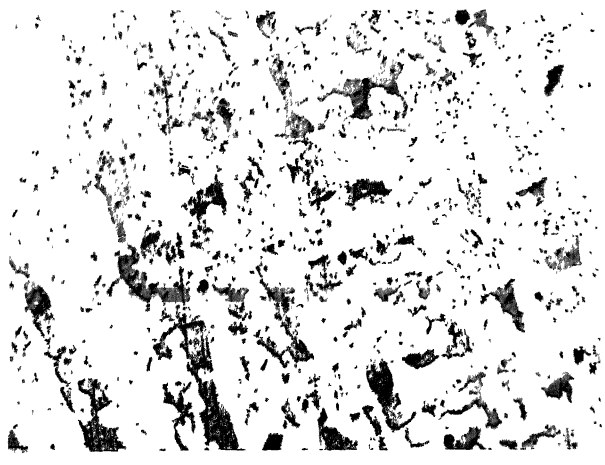

Fig.IV.5b : Microstructure of alloy C_{17}(a) shows 2 phases: matrix-2:17; gray phase-X. (1500 x)

Fig.IV.5c : Microstructure of alloy C_6(a) shows 3 phases: matrix - 2:17; gray phase-X; white regions-γ. (1500 x)

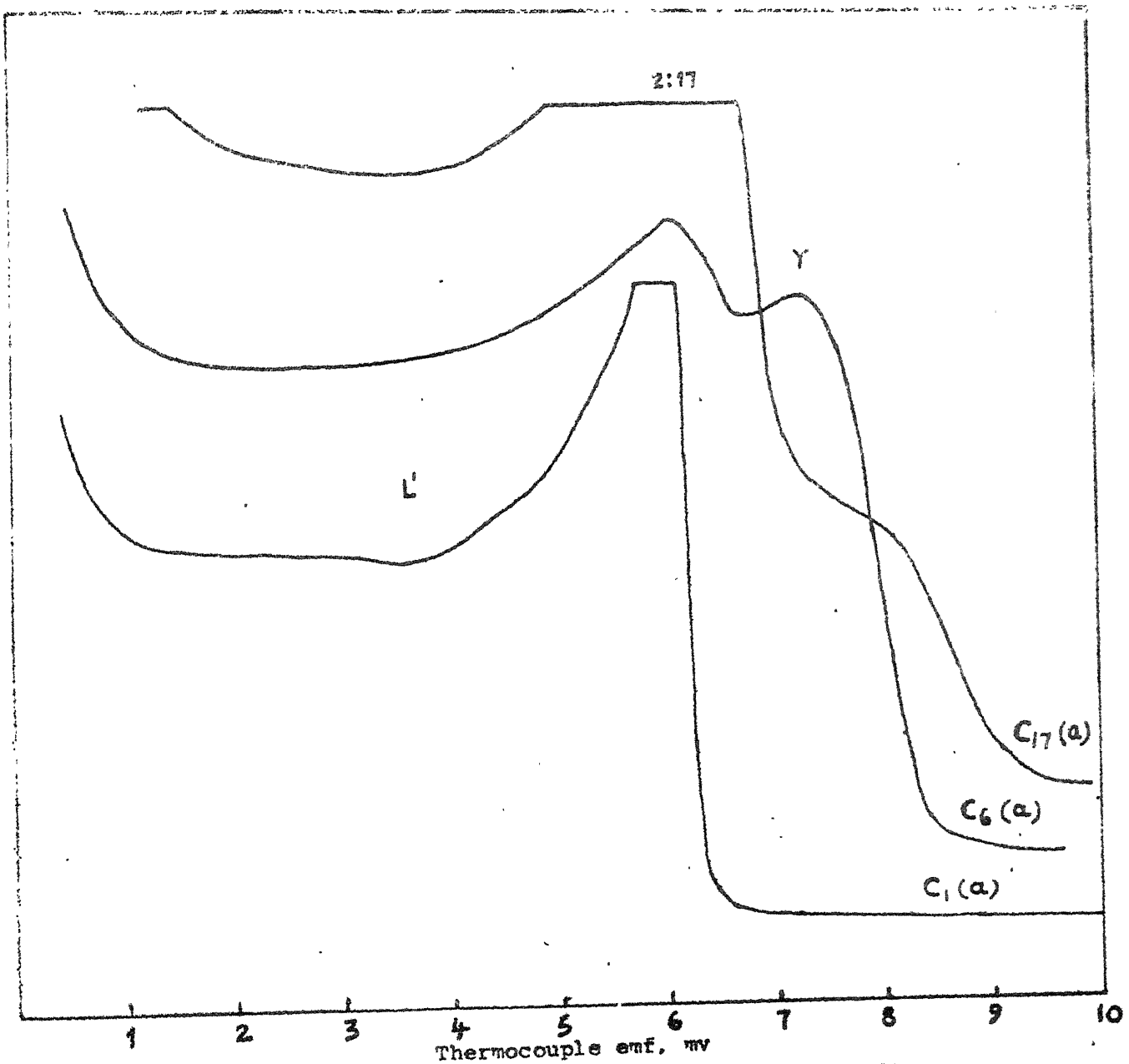

Fig.IV.6 Permeability vs temperature traces for RE-Co-Fe-Cu alloys (C_1(a), C_6(a), C_{17}(a)).

Table IV. 1 : Phase Analysis of 1100°C Annealed (2 days) RE-Co-Fe Cu Alloys

Alloy	Composition, at.pct.				Metallography	X-ray Diffraction Studies	Curie Temperatures, °C		
	Fe	RE	Co	Cu			2:17	fcc	Liquid Phase
C_1(a)	17	17.25	57.75	8	2 phases	2:17 + L'	816	-	-
C_6(a)	17	10	65	8	3 phases	2:17 + X + γ	746	994	-
C_{17}(a)	11.75	12.25	68	8	2 phases	2:17 + X	816	1003	-

X - unidentified phase .

Table IV.2 : Indexed Pattern of 2:17 Phase in Alloy C_6(a). Lattice Parameters a_o=8.430; c_o = 12.289^6 ; c_o/a_o = 1.46.

Line No.	Relative Intensity	d_{obs}, A°	h	k	l	d_{cal}, A°
1	W	3.509	2	0	1	3.499
2	W	3.150	2	0	2	3.138
3	S	2.950	1	1	3	2.937
4	W	2.841	1	0	4	2.832
5	W	2.705	2	1	1	2.692
6	W	2.530	2	1	2	2.517
7	VW**	2.493	1	1	4	2.483
8	S	2.448	0	0	5	2.458
9	S	2.361	2	0	4	2.350
10	VW**	2.150	1	1	5	2.123
11	VS	2.119	2	2	0	2.107
12	VVS	2.101	3	0	3	2.092
13	VVS	2.099	2	2	1	2.077
14	M+	2.059	2	1	4	2.053
15	S	2.054	0	0	6	2.048
16	M+	2.047	2	0	5	2.039
17	W	2.026	3	1	0	2.025
18	VVW**	1.926	3	1	2	1.923
19	VVW**	1.906	3	0	4	1.908
20	S	1.883	2	2	3	1.874
21	W	1.848	1	1	6	1.842
22	VW	1.840	2	1	5	1.835
23	VVW**	1.813	3	1	3	1.815
24	VVW**	1.809	4	0	1	1.805
25	VW**	1.757	0	0	7	1.756
26	VVW	1.712	1	0	7	1.707
27	VVW	1.667	4	0	3	1.667

Continued..

Table IV.2 (Continued):

Line No.	Relative intensity	d_{obs}, A°	h	k	l	d_{cal}, A°
28	VW**	1.623	1	1	7	1.621
29	VW**	1.573	4	1	1	1.580
30	M⁻	1.492	1	0	8	1.503
31	W	1.487	4	1	3	1.485
32	M⁻	1.478	2	1	7	1.481
33	M⁺	1.474	3	2	4	1.470
34	W	1.413	1	4	4	1.414
35	VVW**	1.390	3	3	1	1.396
36	VVW**	1.357	4	0	6	1.363
37	M	1.335	1	4	5	1.337
38	M⁻	1.333	3	3	3	1.329
39	VVW**	1.310	1	5	0	1.311
40	VW**	1.302	5	1	1	1.304
41	VVW**	1.289	3	2	6	1.297
42	W	1.265	4	0	7	1.265
43	W	1.262	2	4	4	1.259
44	M	1.223	3	1	8	1.224
45	M⁻	1.221	3	3	5	1.220
46	W	1.217	6	0	0*	1.217
47	M⁻	1.212	1	0	10*	1.212
48	W**	1.209	6	0	1	1.211
49	VW	1.207	1	5	4	1.206
50	VVW**	1.199	4	3	0	1.200
51	M⁺	1.195	3	4	1	1.194
52	M	1.193	6	0	2	1.194

** Diffraction line is weak and broad.
* Diffraction lines taken for lattice parameters calculation.
Relative Intensity Scale: VVS = Very very strong; VS = Very strong; S = Strong; M = Medium; W = Weak; VW = Very weak; VVW = Very very weak.

similar features as that of the RE-Co-Fe system which means Cu when added in ~8 at. pct. does not change drastically the phases present in the RE-Co-Fe system. When Zr is added in small quantity (2 at. pct.) it has completely changed the phase equilibria, the 2:17 type of ternary phase is not present at all in the RE-Co-Fe-Cu-Zr system and in its place two new phases, one of higher Fe content and the other of lower Fe content are present.

Stress induced $\gamma \longrightarrow \alpha$ phase transformation was not present in RE-Co-Fe system. But the stress induced phase transformation has been found in the case of RE-Co-Fe-Cu system. X-ray diffraction pattern of as powdered alloy C_6(a) has, apart from a 2:17 phase, a fcc (γ) and a bcc (α). The lattice parameter of the fcc phase has been found to be 3.559 A° and that of the bcc phase is 2.845 A° (based on 110 reflection). The bcc phase vanishes when the powder is annealed at 1100°C.

IV.C. Magnetic Characteristics of the RE-Co-Fe-Cu-Zr Alloys

Alloys with Sm : transition metal ratio of ~1:7 have been found magnetically hardenable through low temperature heat treatment. Hence most of the literature available on Zr added RE-Co-Fe-Cu alloys are with Sm. The magnetic characteristics of the MM-Co-Fe-Cu-Zr alloys are not available in the literature. Hence, in this investigation some of the magnetic characteristics of the RE-Co-Fe-Cu-Zr alloys have been obtained. The magnetic characteristics determined are (i) magnetic transition temperatures of phases present in alloys; (ii) susceptibility of the

RE-Co-Fe-Cu-Zr alloys to magnetic hardening treatment and determining approximate heat treatment temperature and (iii) determination of some process parameters for magnet fabrication. These aspects of the study are discussed in the following sections.

IV.C.1 Magnetic Transition Temperatures

Determination of magnetic transition temperature (T_c) has been discussed in Chapter II and the results obtained have been used in analysis of phases present in various alloys to get a positive identification of various phases. Since all the alloys were multiphase and that the magnetic transition curves of the various phases overlapped with each other, the permeability traces were useful for phase analysis only but not for accurate determination of the magnetic transition temperatures. Since the magnetic transition temperatures of all the alloys were $\geq$ 500°C the vibrating sample magnetometer could not be used for T_c determination. The results of the permeability vs temperature traces [Figs. III.5a to d] could be, however, used to determine approximate transition temperature of the γ, U and N phases. Since the γ phase ductile particles could be sieved out, these particles after annealing could be used for magnetic transition temperature determination. The T_c for γ phase of alloy C_{19} appears to be ~ 1047°C (~9.85 mv relative to room temperature 28.3°C). Since alloy C_{18} contain γ phase the second magnetic transition is due to the U phase only. T_c for the U phase from this permeability vs. temperature trace of alloy C_{18} appears to be ~832°C (~7.55 mv relative to room temperature 23.3°C). The U phase T_c was however

found to have a variation with alloy composition as may be seen for the alloys series C_1 through C_{13} which do not contain the N-phase. The lower temperature magnetic transitions (~505°C,~644°C) in this series of alloys is due to L' which can be seen also for the alloys with 13 at. pct. Fe and more prominently for the alloys with 11 at. pct. Fe. The alloy C_{15} did not have any U phase and hence the higher temperature magnetic transition in this alloy is due to the N phase. T_c for the N phase is ~739°C (~6.5 mv relative to room temperature 30°C).

IV.C.2 Effect of Aging Treatment of Bulk Specimens

In Sm-Co-Fe-Cu-Zr system alloys with rare-earth: transition metal ratio of around 1:7 has been found magnetically hardenable through suitable heat treatment. No such study has been made with the MM-Co-Fe-Cu-Zr alloys. To determine which alloy composition is most suited for detailed study of improvement of coercivity, seven alloys with the ratio of transition metal atoms to rare-earth atoms varying between 6:1 to 8:1 (alloys C_{13}, C_4, C_7, C_9, C_{11}, C_{16} and C_{17}) have been subjected to low temperature aging treatment. A small piece of a chosen alloy, annealed at 1100°C, was sealed in evacuated fused silica tube and isothermally annealed at 675°C for various lengths of time. After each predetermined annealing time period the alloy was quenched and $_iH_c$ was determined using a VSM. The results for 675°C aging treatment for all alloys investigated are shown in Fig.III.6. It is clear from the Fig.III.6 that the most promising alloy for aging treatment is the

alloy C_{11}. The 675°C annealing of the C_{11} alloy produced a 15 fold increase in coercivity in about 40 hr. Most of the other alloys, except C_{16} and C_{11}, showed low coercivity even after 60 hr. annealing and C_{16} showed a drop in coercivity after ~32 hr. annealing. The alloy C_{11} showed no decrease in $_iH_c$ upto 48 hr. annealing even though it also showed a drastic decrease in the rate of rise in $_iH_c$ with time. The C_{11} and C_{16} alloys contain basically N phase with only small amounts of second and third phases. High coercivity for both of them indicates that among the phases present in the investigated RE-Co-Fe-Cu-Zr alloys only the N phase responds to the aging treatment.

In order to determine whether further improvement in coercivity is possible through a proper choice of aging temperature, the alloy C_{11} was subjected to two more aging treatments, one at 650°C and the other at 620°C. There was considerably more increase in $_iH_c$ due to aging at 650°C but this test had to be abondoned due to discontinuity in test produced by power failure and it also showed signs of saturation in $_iH_c$ with time. The 620°C aging curve of alloy C_{11} is shown in Fig.III.7. As expected, the aging time required increased considerably due to the choice of a lower temperature. This low temperature aging, however, produced a vast improvement in $_iH_c$ (> 50 times) in about 350 hrs. of annealing. Moreover, the alloy did not show any sign of saturation of $_iH_c$ even after the long annealing. In order to see whether the results are reproducible another piece of alloy C_{11} was annealed at 620°C and $_iH_c$ was measured after 100,223,336 and

466 hrs. of anneal. The results of the second test are shown in Fig.III.7, indicate that $_iH_c$ is reproducible. Thus it appears that the alloy C_{11} at 620°C produces considerably high coercivity in about 300 hr. of aging and no saturation in $_iH_c$ occurs even after a 466 hr.anneal. The microstructure of alloy C_{11} after 350 hr of aging is shown in Fig.III.8a. There is practically no difference between the two micro-photographs,Fig.III.8a,b. Since aging increases the coercivity of the alloy, it may be expected that there is a precipitation of some phase causing an increase in $_iH_c$. No fine precipitate could be observed under optical microscope except segregation of α phase at a magnification of 1500 X. It may mean that the precipitates are too fine and could not be resolved under an optical microscope. Fig.III.7 shows also that there is practically no variation of M_s with aging time. There is 18.5 fold increase in M_r/M_s value after 291 hours of aging (from 0.02 to 0.37). Though the demagnetisation curve is tending to attain squareness,the final M_r/M_s (0.37) value is not promising.

IV.C.3 Effect of Comminution

Ideally a magnet formed with fine powder with single domain particles having no surface damage is expected to show maximum $_iH_c$. This ideal situation, however, can not be achieved. In realistic cases during milling, as the grinding time increases the average particle size becomes smaller and particle size distribution becomes narrower but surface damage of particles increases. With decrease in particle size the susceptibility of

oxidation of powdered material also increases. Thus high value of $_iH_c$ depends on the critical size and size distribution of the powder material. In practical one need not determine the actual average particle size and the size distribution because these determinations require considerable time. In order to reduce time for these studies for a given milling operation one may measure $_iH_c$ as a function of milling time to find the grinding time that produces best value of $_iH_c$. It has been established (35) that narrower particle size is produced in a shorter time if a rod mill is used. Hence, in this study the critical grinding time was determined for rod milling of alloy C_{11}.

To find the critical time of grinding for the alloy C_{11} (annealed at 1100°C), $_iH_c$ was measured as a function of milling time using resin bonded, magnetic field aligned specimens. Fig.III.9 and Table III.7 are showing the variation of $_iH_c$ with milling time for alloy C_{11}. The Fig.III.9 shows that with increase in grinding time $_iH_c$ increases. Within reasonable period of grinding (upto 6 hr) $_iH_c$ was found to increase steadily. Since usually for RE-Co-Fe alloys 3 to 4 hr.rod milling produces very fine powder no further grinding of the alloy was done even though $_iH_c$ did not show a tendency to decrease. Critical particle size and particle distribution could not be measured due to shortage of time.

The steady increase in $_iH_c$ value for 6 hrs grinding is because of proper alignment of particles as they approach single

domain particle character. M_r/M_s is high (= 0.53) in fine particle state as compared to the bulk form (M_r/M_s = 0.02) at room temperature. M_r/M_s, however, appears to remain almost constant with reduction in particle size. M_s value is slightly high in resin bonded magnets compared to that of the bulk specimens. This indicates that 10 KOe field strength used for initial magnetisation of bulk specimen is not quite sufficient to cause full magnetic saturation.

CHAPTER V

CONCLUSIONS

On the basis of the results of investigations pertaining to phase equilibria in the RE-Co-Fe-Cu-Zr system at 1100°C and magnetic characterisation studies of the 1100°C annealed alloys the following conclusions can be drawn.

(i) From the phase analysis of the investigated region of the system RE-Co-Fe-Cu-Zr with fixed amounts of Cu (8 at. pct.) and Zr (2 at. pct.), entirely different sets of phases became stable compared to the RE-Co-Fe alloy system.

(ii) New quinary phases U phase and N phase are found as major phases in the investigated region. There are other phases in small amount which could not be indexed.

(iii) The limited investigation does not allow exact location of liquid, U, N and γ phase regions. However it indicates the locations in the phase diagram at which these phases may be found.

(iv) U phase is a high Co containing phase and is located somewhere at the high Fe contents > 19 at. pct. This phase can be indexed on the basis of a hexagonal cell with the lattice parameters, a_o = 5.907 A° and c_o = 33.324 A°, c_o/a_o = 5.64.

(v) The γ phase has been identified as the fcc Co solid solution located at the Co end of the RE-Co-Fe-Cu-Zr system.

(vi) Liquid phase exists at 1100°C at the high RE content side of the diagram.

(vii) N phase is located at a lower Fe content (< 11 at. pct. Fe) towards the left hand corner of the investigated region and it is not found above 13 at. pct. Fe.

(viii) From the very limited work done in RE-Co-Fe-Cu system, it is found that it is showing basically similar features as that of the RE-Co-Fe system which means Cu when added in ~ 8 at. pct. does not change drastically the phases present in the RE-Co-Fe system.

(ix) When Zr is added in small quantity (2 at. pct.) it changes completely the phase equilibria; the 2:17 type phase of the RE-Co-Fe or RE-Co-Fe-Cu systems is not at all present in the RE-Co-Fe-Cu-Zr system.

(x) Stress induced $\gamma \rightarrow \alpha$ phase transformation was not present in RE-Co-Fe system. But stress induced phase transformation has been found in the case of RE-Co-Fe-Cu and RE-Co-Fe-Cu-Zr systems at higher Co and higher Fe ($\geq$ 16 at. pct.) levels.

(xi) Lattice parameters of the γ phase in RE-Co-Fe-Cu-Zr system is a_o = 3.562 A°. The lattice parameter of the γ phase in RE-Co-Fe-Cu system is a_o = 3.559 A°. This may suggest that addition of Zr does not change the lattice parameter of the γ phase in a significant way. Similarly lattice parameters of stress induced α phase (bcc) is same in both RE-Co-Fe-Cu and RE-Co-Fe-Cu-Zr systems (a_o = 2.845 A° for alloy C_6(a) and a_o = 2.846 A° for alloy C_6). Possibly it

means the solubility of Zr in Co fcc solid solution is very less.

(xii) The addition of Cu lowers T_c of 2:17 phase.

(xiii) T_c of the new intermediate phases U and N are quite high ~860°C and ~723°C, respectively.

(xiv) N phase alloys (C_{11} and C_{16}) appears to respond to the aging treatment compared to the U phase alloys.

(xv) There is > 50 fold increase in $_iH_c$ value in about 350 hrs. of aging of alloy C_{11} at 620°C. There is practically no variation of M_s with aging time. M_r/M_s has increased by about 18 times.

(xvi) $_iH_c$ increases with increase in grinding time (decrease in size) even after 6 hrs. of grinding. $_iH_c$ did not show a tendency to decrease after 6 hrs. milling.

REFERENCES

(1) B.D. Cullity, "Introduction to Magnetic Materials", Addison-Wesley Publishing Company, Massachusetts, 556 (1972).

(2) K.J. Strnat, G.I. Hoffner, J. Olson and W.Ostertag, J. Appl. Phys., 38, 1001 (1967).

(3) E.A. Nesbitt, H.J. Williams, J.H. Wernick, and R.C.Sherwood, J. Appl. Phys., 33, 1674 (1962).

(4) E. Tatsumoto, T. Okamoto, H. Fujii, and C. Inove, J. de Physique, 32, C1-550 (1971).

(5) T. Ojima, S. Tomizawa, T. Yoneyama, and T. Hori, IEEE Trans. Magn. 13, 1317 (1977).

(6) E.A. Nesbitt, R.H. Willens, R.C. Sherwood, E. Buchler, and J.H. Wernick, Appl. Phys. Letters, 12, 361 (1968).

(7) K.H.J. Buschow, J. Less Common Metals, 16, 45 (1968).

(8) A.E. Ray, and K.J. Strnat, "Goldschmidt Informiet", 4/75, Nr. 35 (1975).

(9) E.A. Nesbitt, G.Y. Chin, R.C.Sherwood, and J.H. Wernick, J. Appl. Phys., 40, 4006 (1969).

(10) H.J. Leamy, and M.L. Green, IEEE Trans. Magn., 9, 205 (1973).

(11) G.Y. Chim, M.L. Green, and H.J. Leamy, AIP Proc., 24, 691 (1975).

(12) Y. Khan, J. Less Common Metals, 34, 191 (1974).

(13) A.E. Ray, A.T. Biermann, R.S. Harmer and J.E. Davison, Cobalt, No. 4, 103 (1973) and A.E. Ray, Cobalt, No.1, 13 (1974).

(14) K.P. Gupta, "Science and Technology of Rare Earth Materials", Academic Press, New York (1982).

(15) K.H.J. Buschow, Phys. Stat. Soli., 7, 199 (1971).

(16) G. Schafer, and W. Spyra, Forschungsbericht, T 76-37, Zentralstelle fur Luft-und Raumfahrtdokumentation und information, Munich (1976).

(17) E.M.T. Velu et al, J. Less Comm. Metals, 71, 219 (1980).

(18) R.C. Mittal et al, J. Less Common Metals, 78, 245 (1981).

(19) S. Laha et al, (to be published) (Private communication).

(20) A.J.Perry, J. Less Common Metals, 51, 153 (1977).

(21) E.M.T. Velu, Ph.D. Thesis, IIT Kanpur (1981).

(22) J.W. Walkiewiez, and M.M. Wong, IEEE Trans. Magn., 15 (1979).

(23) T. Yoneyama, A. Fukuno and T. Ojima, "Rare Earth-Cobalt Permanent Magnets and their Applications", Proc. Conf. Hakone, Japan, 407 (1979).

(24) T. Nezu, M. Tokunaga, and Z. Igarashi, "Rare Earth-Cobalt Permanent Magnets and their Applications", Proc. Conf. Hakone, Japan, 437 (1979).

(25) M.P. Arbuzov, A.A. Pavlyukov, and E.I. Gilkhman, Fiz. Met. Metalloved,58, 688 (1984).

(26) J.W. Walkiewicz, J.S. Winston and M.M. Wong, Bureau of Mines (Pamphlet), Washington DC, No. 8583, 12 (1981).

(27) R.K. Mishra, and G. Thomas, J. Appl. Phys., 52, 2517 (1981).

(28) H. Nagel, J. Appl. Phys., 50, 1026 (1979).

(29) J.J. Becker, Rep. Nav. Res. off. SRD-77-081 (1977).

(30) J.D. Livingston and D.L. Martin, J. Appl. Phys., 48, 1350 (1977).

(31) H. Yaofu, and S. Guangfei, Vth Int. Workshop on Rare Earth-Cobalt Permanent Magnets and their Application, Roanoke, Virginia (1981).

(32) D.K. Das, IEEE Trans. Magn. 5, 214 (1969).

(33) M.G. Benz and D.L. Martin, Appl. Phys. Letters, 17, 176 (1970).

(34) V. Manuja, M. Umadevi and K.P. Gupta, Int. Conf. Progress in Met. Research: Fundamental and Appl. Aspects, IIT Kanpur (1985) (to be published).

(35) N.R. Bonda, Ph.D. Thesis, IIT Kanpur (1981).

(36) A.E. Paladino, N.J. Dionne, P.F. Weirauch and E.C. Wettstein, Goldschmidt Informiert, Nr 35, 4/75, 63 (1975).

APPENDIX-I

PROCEDURE TO BE ADOPTED IN RUNNING THE CURIE-TEMPERATURE APPARATUS

Before starting the experiment the following connections are to be made:

(i) Thick gray wires from transducer coils (primary) are to be plugged into the 'drive' position (red and black sockets) on the detector system. Ground terminal is to be inserted in the green socket.

(ii) Orange colour wires from transducer coils (secondary) are to be connected to the 'pick up' on the detector system.

(iii) Red and black wires from the output ('recorder') of the detector system are to be connected to the y-axis input terminals of the recorder.

(iv) The top thermocouple wires are to be plugged into x-axis input terminals of the recorder.

(v) Thermocouple wires coming from bottom part (metal-glass joints) of the furnace are to be connected to a digital millivoltmeter.

Once the above connections are made the following steps are to be followed for running the apparatus.

The sample is loaded in a quartz tube specimen holder and kept in side the furnace assembly and all the screws are tightened. The detector system and the recorder are to be

switched on and the following adjustments be made: put 'gain select' switch in position c and y-axis 'range' selector switch on the recorder at 0.5 v/cm. Now move the specimen in and out of the coil. This should show a quick deflection of the recorder pen in y-direction. This indicates that the detector system is working well.

The specimen is first placed at the fully pulled up position, so that the material is far off from the furnace when it being heated up. The rotary pump is switched on. The furnace heating starts only after attaining a vacuum of better than 50 μ Hg pressure. After ensuring water circulation the furnace heating is started, slowly in the beginning for 3 hours. Slow heating rate is obtained by adjusting the input voltage at the rate of 4 volts per half an hour. When the furnace attained ~600°C (at about 25 to 30 v setting) which can be read through a digital millivoltmeter, water circulation for the diffusion pump is to be started and the diffusion pump to be switched on . After attaining a pressure of 1 μ Hg, the heating rate is increased as shown below:

(i) 4 volts per 25 min. for 50 min.

(ii) 4 volts per 20 min. for 60 min.

(iii) 4 volts per 15 min. for 30 min.

Heating in this manner takes four to five hours to heat up the furnace to ~1050°C (at ~52 volts furnace input).

Just before the furnace attains its desired temperature, recorder adjustments have to be done.

(i) a centimeter graph paper is fixed on the recorder with cellotape.

(ii) switch on the recorder power and press in 'chart' button of the recorder.

(iii) press in 'servo' button and see that the bottom push button is in 'set up' mode.

(iv) zero adjustment of x-axis, to be done by first pressing the 'zero check' button (small red button) and simultaneously adjust the x-axis 'zero' adjustment knob to a desired position. This is the room temperature zero position of the recorder. Release the 'zero check' button.

(v) set 0.5 mv/cm on the x-axis selector 'range' of the recorder.

(vi) set the pen at desired position on the chart by adjusting the 'zero' adjust knob for the y-axis.

(vii) The setting given here are for position M of the 'gain select' switch of the detector system.

(viii) If the sample is less than 0.5 grams, set 0.25 v/cm or 0.1 v/cm scales on y-axis can be used. But for samples which weigh between 0.5 to 1 gram, 0.5 v/cm scale is best.

Note: When ever sudden changes are expected to be made about the position of the sample inside the coils, recorder pen should be off and push button should not be in 'record' mode.

After attaining the required temperature of the furnace, the sample is pushed into the furnace. Detector system is switched on. It will take 6-7 min. for the sample to get heated up to the furnace temperature. Just before taking the sample into transducer coils, once again check x-axis zero with 'zero check' knob. Then the sample is pulled up and rested inside the the transducer coils at a predetermined position (a gauge is used to put the sample in the desired position of the transducer coil) at which signal intensity is maximum. Immediately without any delay press 'pen' and push the push button towards 'record' mode simultaneously and the cooling curve is traced. It will take 10-15 min. to record the trace. After this switch off power supply to recorder detector and diffusion pump. Let the rotaory pump run half an hour more with all water circulations to get the oil in diffusion pump cool down, otherwise the oil (hydrocarbons) will crack and its life will go down. Switch off rotaory pump and close all water circulation taps.